Anomalous reaction mean free paths of nuclear projectile fragments from heavy ion collisions at 2A GeV

E. M. Friedlander, R. W. Gimpel, H. H. Heckman, and Y. J. Karant
Nuclear Science Division, Lawrence Berkeley Laboratory, University of California, Berkeley, California 94720

B. Judek
Division of Physics, National Research Council, Ottawa, Ontario, Canada K1A 0R6

E. Ganssauge
Fachbereich Physik, Philipps Universität, D-3550 Marburg, Federal Republic of Germany
(Received 16 August 1982)

We present in detail the description and the analysis of two independent experiments using beams of ^{16}O and ^{56}Fe. From their results it is concluded that the reaction mean free paths of relativistic projectile fragments, $3 \leq Z \leq 26$, are shorter for a few centimeters after emission than at large distances, where they are compatible with values predicted from experiments on beam nuclei. The probability that this effect is due to a statistical fluctuation is $< 10^{-3}$. The effect is enhanced in later generations of fragments, the correlation between successive generations suggesting a kind of "memory" for the anomaly. Various systematic and spurious effects as well as conventional explanations are discussed, mainly on the basis of direct experimental observations internal to our data, and found not to explain our results. The data can be interpreted by the relatively rare occurrence of anomalous fragments that interact with an unexpectedly large cross section. The statistical methods used in the analysis of the observations are fully described.

NUCLEAR REACTIONS ^{16}O and ^{56}Fe at 2A GeV on emulsion nuclei; reaction mean free paths of primary beams and projectile fragments measured and compared.

I. INTRODUCTION AND HISTORY

Observations in nuclear research emulsion that have given provocative evidence for short reaction mean free paths of relativistic projectile fragments of high-energy heavy ions in the cosmic radiation have been reported sporadically since 1954. The first evidence for "anomalous" extranuclear cascading induced by heavy primary cosmic-ray nuclei was given by Milone.[1] Subsequent observations by Yagoda[2] and Tokunaga *et al.*[3] suggested that secondaries and later generations in the cascades might have a mean free path (mfp) five to ten times shorter than the value expected from a geometrical overlap model[4] that was in reasonable agreement with values observed for "primary" nuclei. In 1959 Friedlander and Spirchez[5] examined six cosmic-ray initiated cascades and found a difference between the mfp of "first" and "second" generation fragments. The first systematic studies of the effect were performed by Judek.[6] On the basis of mfp measurements of relativistic cosmic-ray primary and secondary nuclei involving about 1000 interactions, Judek concluded that a few percent of the secondary nuclei with charges $1 \leq Z \leq 4$ interact with anomalous mfp's of the order of 3 cm and that the stars produced by the anomalous particles had the characteristics of "typical" nuclear interactions as observed in emulsion. Evidence for short mfp's for secondary relativistic fragments was also reported by Cleghorn.[7]

Because of limited statistics, possible systematic uncertainties, and the implausibility (even impossibility) of such a nuclear component within known

nuclear physics, these enigmatic observations have never been widely recognized nor accepted. In 1972 Judek exposed nuclear emulsions to the 2.1A GeV ^{16}O beam of the Bevalac and obtained a partial confirmation of her earlier cosmic ray results.[8] The aim of the present collaborative Bevalac experiment was to obtain sufficient statistics to decide whether there is evidence for a short mfp for projectile fragments (PF's) emitted from the interactions of $\sim 2A$ GeV (Ref. 9) ^{16}O and ^{56}Fe beams with target nuclei in nuclear track emulsions. Our results provide this evidence.

A summary of our results, based on a total of 1460 interactions of PF's in emulsion stacks exposed to Bevalac beams, independently scanned and measured at the National Research Council (NRC) of Canada and Lawrence Berkeley Laboratory (LBL), is as follows[10]: (a) Over the first few centimeters after emerging from a nuclear interaction (~ 10 g/cm^2 of matter traversed or, equivalently, $\sim 10^{-11}$ s proper time) the PF's exhibit significantly shorter mfp's than those derived from "normal" beams of the same charge Z; (b) at larger distances from the emission point, the mfp's revert to values compatible with those for normal beam nuclei; and (c) the observations are not compatible with a homogeneous lowering of the mfp and require the presence of at least one component with an unexpectedly high reaction cross section.

Since our first communication on this subject,[10] results of two independent experiments[11,12] have shown essential agreement with these conclusions. The emulsion technique and the results derived therefrom on primary beams are well established.[13,14] The basic method we have used is known as the *along-the-track* scan, where one simply follows each track until it either interacts or exits the detector. An interaction in such a scan is defined to be the emission of at least one charged hadronic track, either from the projectile or the struck target nucleus in the emulsion. Preceding experiments have yielded by this method the mfp's of primary beam nuclei to a statistical precision of $\sim 3\%$. Specific to this result, mfp's for ^{4}He, ^{12}C, ^{14}N, and ^{16}O had been obtained at LBL (Ref. 15) and for ^{16}O at NRC.[8] As part of the present experiment, mfp's for primary ^{40}Ar and ^{56}Fe were measured at LBL and for ^{4}He and ^{56}Fe at NRC. The primary beam mfp measurements were done in all cases at about 2A GeV, with some measurements also performed at lower energies to obtain information on energy dependence. We found no such dependence within the accuracies of our measurements. As will be shown, the 2A GeV primary beam measurements are in good agreement with the measurements on PF's beyond about 5 cm from their points of emission. Below this distance, we observe significant and regular deviations from both the primary beam measurements and the "large distance" observations. Further, the results of the two independent observations concerning PF's from ^{56}Fe at LBL and ^{16}O at NRC are in agreement.

This paper is organized into six sections. In Sec. II we discuss what one would reasonably expect to be the reaction properties of PF's based on known nuclear physics. Section III describes the techniques used in this experiment and the systematics they imply. In view of the potential importance of our results it is necessary for us to examine in detail several subsets of the data. By necessity, these subsets, having qualitatively different responses to various systematic or spurious effects, also have a different statistical behavior. For these reasons, Sec. IV presents the formal statistical methods needed to analyze the data in a cogent fashion with mathematical details given in Appendices A and B. Section IV also includes a discussion of the Monte Carlo simulations used to test the formalism and its physical approximations in light of the material given in Secs. II and III. Section V and Appendix C describe the results using the methods of Sec. IV, and Sec. VI summarizes the conclusions of the investigation. A note on notations: Asterisks (*) will refer to *estimates,* overbars to *sample averages,* and angular brackets $\langle\ \rangle$ to *expectation values.*

II. BASIC CONCEPTS AND EXPECTATIONS

To deem that an observation is anomalous, one must first establish normality. In the present case, we need to know the normal interaction behavior of nuclei in emulsion, particularly nuclei of kinetic energy between 1.5 and 2A GeV. This is given in its simplest form by the total (or inclusive) reaction mfp, denoted by λ. While the measurement techniques and the statistical properties of various estimates for λ will be discussed later, the mfp has a simple physical interpretation in terms of number densities of target nuclei and cross sections, namely:

$$\lambda = \left[\sum_{i=1}^{k} n_i \sigma_{\text{obs}}^i \right]^{-1} . \tag{1}$$

Here k is the number of different nuclides in the emulsion, n_i is the number of nuclei per unit volume of nuclide "i" (Ref. 14), and σ_{obs}^i is the cross section for the projectile to interact in a visually observable manner with component i. The cross sec-

tion σ_{obs} is defined to include the detection efficiency. Note that a large σ_{obs} corresponds to a short λ. However, because emulsion is a heterogeneous mixture of elements, one necessarily measures λ, not σ_{obs}. Nonetheless, a knowledge of the properties of λ carries over to information about σ_{obs}.

To an excellent approximation, the σ_{obs}^{i}'s in question are just a constant fraction of the total reaction cross section. Two properties of heavy ion reaction cross sections are important here: From about $0.5A$ GeV to $\gtrsim 2A$ GeV, (i) the σ_{obs} are essentially constant and (ii) they are well described by a geometrical dependence.[16]

In its simplest approximation, the geometrical dependence of the reaction cross section is expressed in the Bradt-Peters form,[4]

$$\sigma_{12}=\pi r_0^2(A_1^{1/3}+A_2^{1/3}-\delta)^2 , \tag{2}$$

where r_0 and δ are constants and A_1 and A_2 are the baryon numbers of target and projectile. If

$$A_1^{1/3} \gg A_2^{1/3}-\delta ,$$

then $\sigma \propto A^{2/3}$.

Because $A \propto Z$ near the valley of stability (VOS), one might roughly expect that $\sigma \propto Z^{2/3}$ with the same restriction as above. This suggests a more general relationship of the form

$$\lambda=\Lambda Z^{-b} . \tag{3}$$

In fact, Eq. (3) adequately fits the primary beam data, with $b \approx 0.4$.

The equations to be solved for estimating Λ and b are presented in Sec. IV. Using these, one obtains two fits, one for NRC, the other for LBL.

At NRC: $\Lambda^*=28.9\pm2.5$ cm, $b^*=0.43\pm0.04$. At LBL: $\Lambda^*=32.2\pm2.5$ cm, $b^*=0.44\pm0.03$. While the consistency of the observations is evident, we stress that these are measurements of beam nuclides limited to the VOS.

It is evident that not only VOS nuclides are present among the PF's but also isotopes away from the VOS, as well as various excited states with lifetimes $c\tau \gtrsim 1$ cm. To incorporate the deviations these effects might produce in the mfp's (which are really a function of Z, A, and the quantum state) one has two alternatives. The first, obviously, is to measure empirically all these mfp's. It is equally obvious that the logistics of such a measurement would be intractable. The second alternative, albeit somewhat less secure, is to obtain calculated values of mfp's based on realistic models[17] that use other experimental data, such as form factors and detection efficiency. This we have done. The results are displayed in Fig. 1, along with the experimental observations and a power-law fit to these data.

The small circular points in Fig. 1 are the calculated values of $\lambda(Z)$ for nuclei of charge Z at $2A$ GeV in emulsion obtained from Karol's "soft-spheres" model.[17] The mfp measurements on primary beams at $2A$ GeV, indicated by the large circles and triangles, are well represented by the calculations, assuming the values of the parameters used in the Karol formalism given in Ref. 15. In several cases the multiple values of the mfp at the same Z illustrate the dependences of $\lambda(Z)$ on the isotopic mass A of the projectile. The straight line is the fit to the combined LBL-NRC data sets, $\lambda(Z)=30.4Z^{-0.44}$ cm. While the general trend is reproduced, there does appear to be a theoretical prediction that the mfp's for the $Z=3,4,5$ isotopes will fall below the fitted lines.[18] Additionally, isotopic "noise" is visible. In Sec. IV C, which concerns the Monte Carlo simulations of the experiment, the methodology for dealing with these aspects of the mfp's will be examined.

III. METHOD OF OBSERVATION AND SYSTEMATICS

In this section, three main points will be discussed: (i) the quantities measured, (ii) how the measurements were conducted, and (iii) the problem of systematic errors posed by these measurements.

(i) Beams, stack characteristics, and scanning procedures. Two stacks of Ilford G-5 nuclear research emulsion pellicles, nominally 600 μm thick, were

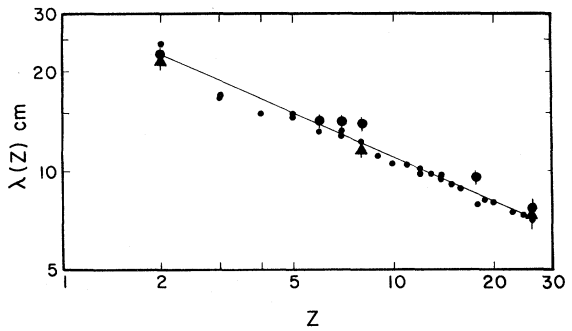

FIG. 1. The mean free path $\lambda(Z)$ vs Z. The large circles with error bars are the LBL observations on primary beams; the large triangles with error bars are the NRC primary observations. The small circles are theoretical predictions normalized to primary beam data; the appearance of multiple circles for the same Z represents isotopes of different A. The straight line is $30.4Z^{-0.44}$ cm, which represents the average fit to both data sets combined.

exposed at the Bevalac to relativistic heavy ion beams parallel to the emulsion surfaces. Stack I, 50 pellicles, of size 15×30 cm^2, was exposed to 2.1A GeV ^{16}O and scanned and measured at NRC. Stack II, 42 pellicles of size 7.5×12 cm^2, was exposed to 1.88A GeV ^{56}Fe and scanned and measured at LBL. The track densities of the ^{16}O and ^{56}Fe beams were ~5 and $\sim3\times10^3$ cm^{-2}, respectively. The stacks were processed separately at LBL. A 1-mm^2 grid was photographed on each pellicle before the latter was removed from its respective stack, mounted on glass, and processed.

At both NRC and LBL, an unbiased forward "along-the-track" scan was used. This means that a primary track was picked up on a scan line as it entered the stack; this scan line was 2 mm from and parallel to the leading (milled) edge of each pellicle in the Fe stack, and at 5 mm in the O stack. The track was examined to ensure that it did not interact before the scan line. The Fe primaries were followed until they either interacted or left the pellicle; the O primaries were followed until they interacted or left the stack. When the primary interacts, any PF produced is called a secondary. When a secondary PF interacts, any PF produced is a tertiary, and so on. An example of a primary-secondary-tertiary "two-link chain" event is shown in Fig. 2. All PF's of $Z\geq3$, regardless of generation (secondary, tertiary, . . . ,), were followed until they interacted or left the stack.

Table I summarizes the data base for this experiment, giving the number of interactions observed for the primary ^{16}O and ^{56}Fe beams and for projectile fragments versus generation. Projectile fragments, as indicated by their name, are nuclei produced at low velocities in the projectile frame. Hence at $\gamma\simeq3$ they are emitted in a narrow forward angular cone having velocities essentially that of the projectile. The average momentum shift in the laboratory frame of a PF relative to its parent is only on the order of -150 MeV/c at $\simeq3A$ GeV/c,[19] a momentum, i.e., energy, loss that is smaller than that caused by ionization in the emulsion. We shall examine this point in the discussion of the energy spectra of the PF's (Sec. VI B 4). At the energies used in this work, PF's of $Z\geq3$ are confined to a forward cone that is characterized by the Fermi momentum of the fragments within the projectile nucleus.[19] We accepted PF's within the forward 6° cone, with all angular measurements being corrected for the shrinkage in the thickness of the processed pellicles.

In this experiment an interaction ("star") was defined as the emission of at least one (observable) charged hadronic track at the vertex in addition to the fragment under investigation. At LBL the dis-

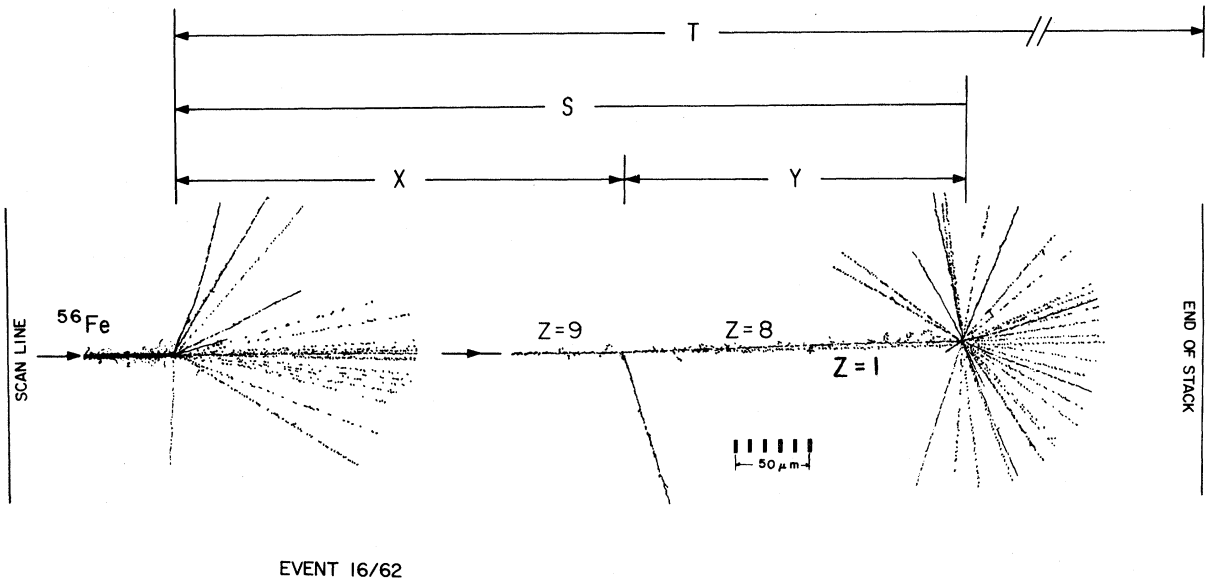

FIG. 2. Microprojection drawing of an interaction of a 1.88A GeV ^{56}Fe nucleus in emulsion. This primary star produced a two-link chain of PF interactions. The $Z=9$ secondary PF travels a distance $X=2.6$ cm before interacting, giving rise to a $Z=8$ tertiary PF that interacts after traveling a distance $Y=0.02$ cm, as well as a $Z=1$ PF (not followed). The total length of the chain is S, and the potential path length T is the distance available for the complete chain to develop. The longest chain in the data (from ^{16}O) included seventh generation PF's. The variables X, Y, S, and T are defined here for use in Secs. IV B and V C.

TABLE I. Numbers of observed interactions. ^{16}O data are from NRC, ^{56}Fe from LBL.

Primary beams	^{16}O	^{56}Fe	Total
	1460	946	2506
Projectile fragments, $Z \geq 3$ Generation			
2	609	590	1199
3	101	121	222
4	16	18	34
5	2	1	3
6	1		1
7	1		1

tances were estimated to 100 μm by use of the 1 mm^2 grid imprinted on the pellicles, the grid being checked by microscope-stage coordinates. At NRC the stage coordinates were used directly, with a verification of distances obtained from the grid coordinates.

All data at LBL were rescanned by a different observer using a somewhat different technique from the initial scan. Since one could imagine the potential pitfall of differential scanning efficiency (a scanner being more observant immediately following a vertex), the scanners backscanned all interacting PF's proceeding backward from all observed interaction vertices, and forward rescanned all noninteracting PF's from their emission point.

At NRC, searches for charge-changing interactions missed in scanning were conducted by repeated charge measurements along the track. The charges of all primary nuclei were determined at the interaction vertex, or, in the case of noninteracting tracks, at about 5 mm from the exit edge of the stack. The charges of PF's were determined near their emission vertex as well as at the next interaction vertex, if they interacted, or at the exit point from the stack if no interaction was detected. If any charge change was observed, the tracks were carefully rescanned for the missed interaction. This naturally increased the detection efficiency for certain classes of stars at NRC relative to LBL, namely stars with a small charge change to the next generation PF. In both experiments, the scanning was done under $\simeq 500\times$ magnification, with questionable vertices examined under higher power, where spatial resolution of $\lesssim 1$ μm is obtainable. We defer discussion of certain potential vertex misidentification and background problems to Sec. VI.

(ii) *Charge measurements.* Because the mfp of a nuclide is a function of its baryon number A, and hence Z, charge measurements via mean gap length and δ-ray densities were carried out for PF's $Z \geq 3$. The measurements of charge of the PF's in this experiment were greatly simplified by the persistence of (relativistic) beam velocity,[19] which enabled us to assume that the linear density of δ rays of the PF's was proportional to Z^2.

The LBL and NRC groups utilized both δ rays and linear track structure to determine the charges of tracks; their techniques differed in significant details, this difference being primarily attributable to the much higher δ-ray densities of the fragments $Z > 8$ occurring in the Fe stack. For $Z \lesssim 5$, the LBL group estimated charge from the lacunarity L of the track, given by

$$Z \propto (\,|\ln L|\,)^{1/2}\,,$$

where L is the fractional linear transparency of the track.[14] In the range $6 \leq Z \leq 26$, charge was deduced from the "lacunarity" of δ rays, where L is defined to be N_E/N_T, i.e., the ratio of the number of times *no* δ rays are observed in a cell length S (typically 15 μm) to the total number of cells examined. In this technique a δ ray is defined to be one that projects radially a minimum of ~ 1.5 μm from the center of the track.[20]

To determine the reproducibility of the charge measurements, the method of repeated observations was used at LBL. A track was chosen at random that had been first measured to give charge Z_1, say. Subsequent independent observations were made on different segments of the same track, yielding measurements $Z_2, \ldots, Z_N$. The deviations $Z_1 - Z_2$, $Z_1 - Z_3, \ldots, Z_1 - Z_N$ were histogrammed, and since for the different Z_1's the results of $Z_1 - Z_i$ were compatible, one final histogram was produced, Fig. 3 (LBL). This yielded an empirical charge reproducibility of ± 1 charge unit from $6 \leq Z \leq 26$. These deviations were obtained at different depths and in different plates to verify the correction for development gradients and to test the uniformity of the stack. Further, they were examined for a systematic shift with distance into the stack; such a shift could indicate a change in track structure due to a slowing of the fragment. No such shifts were found, lending further credence to the assumption that one was in fact dealing with relativistic PF's.

Two main procedures of δ-ray counting were employed at NRC, the counting of all δ rays (a) with four or more grains and (b) that extended > 1.3 μm from the center of the track. Procedure (a) was used in the early stages of this work. Procedure (b), although more time consuming, gave an improved charge resolution. A track segment of about 5 mm was used for each count, depending on the particle's

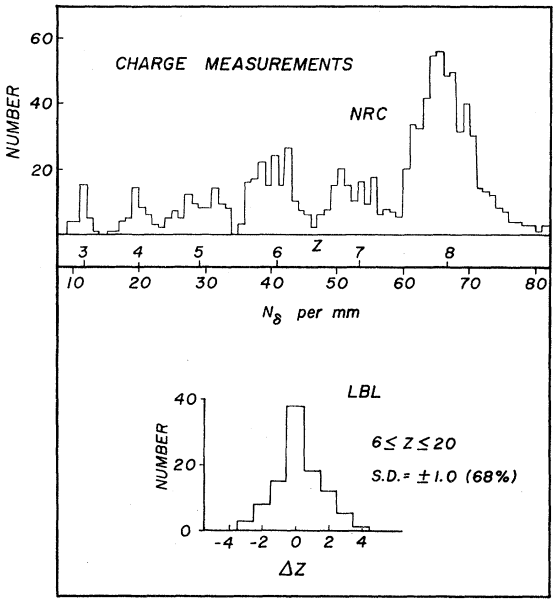

FIG. 3. Histograms of δ-ray density with an added charge scale (NRC) and of charge reproducibility (LBL).

charge. The charge distribution obtained from δ-ray measurements using (b) is given in Fig. 3 (NRC), showing a statistical accuracy of $\frac{1}{3}$ charge unit for $5 \leq Z \leq 8$ and of about $\frac{1}{4}$ charge unit for $Z=3$ and 4. Gap-density measurements were found to give complete charge resolution for $Z=3$ and $Z=4$ in 1 mm of track length.

(iii) *Energy spectrum.* The only technique available in this experiment to measure the energy spectrum of PF's is that deduced from the quantity $p\beta$ resulting from multiple scattering measurements. However, at the energies involved in the current experiment, such measurements are not nearly sensitive enough to provide an accurate energy spectrum. Multiple scattering measurements carried out at NRC provide proof that the PF's were qualitatively in excess of 1A GeV (for $Z/A=\frac{1}{2}$) and entirely consistent with the calculated energy spectrum.

To calculate the energy spectra of the interacting beams and PF's we incorporated several pieces of information. (i) We assumed the values given in the literature for the specific ionization constant.[14] (ii) Spectrometer measurements have shown that the longitudinal momentum distributions of PF's in the laboratory frame are characteristically Gaussian shaped, with mean shift $\langle p_{\|} \rangle \simeq -150$ MeV/c in total momentum and standard deviations typically 450 MeV/c.[19] Let us consider a PF of mass $A=10$ that is emitted from a parent nucleus of total momentum of 25 GeV/c, assuming the persistence of velocity. At the -3 standard deviation level, the PF would be shifted downward by -1.5 GeV/c, or about 6% of its total momentum at beam velocity. In terms of kinetic energy, this is about an 8% degradation. Hence, even in this worst case analysis, we conclude that the effect of kinetic energy/nucleon loss at emission of a PF relative to its parent is small compared to the energy losses caused by ionization in the emulsion.

The resultant calculated energy spectra for the PF's in the experiment utilizing this information are displayed in Fig. 4. As can be seen, none of the PF's would have had an energy below 1A GeV and few below 1.5A GeV.

The important conclusion that comes from this calculation is that, because of the near energy independence of the reaction cross section for energies $E \gtrsim 1A$ GeV,[16] we are assured that the expected mfp's, $\lambda(Z)$, of the PF's are constant, independent of position in the emulsion detectors.

IV. STATISTICS OF MEAN FREE PATH MEASUREMENTS

From its very beginning, the problem of the anomalously short mean free paths of projectile

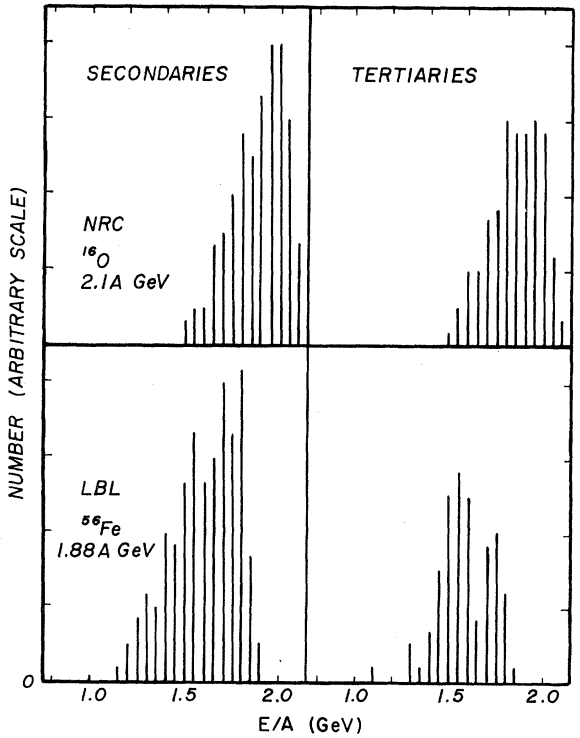

FIG. 4. The calculated distributions of kinetic energies per nucleon in the laboratory frame of PF's for the interactions of ^{16}O (NRC) and ^{56}Fe (LBL) for the second and for the later generations.

fragments has been plagued by the relatively small statistical samples involved, which entailed, to a certain extent, justifiably, a general mistrust about the reality of the effect.

However, samples of arbitrary size are susceptible to exact statistical treatment; this should enable one to extract the maximum amount of information from the data available. The aim of the analysis is to test the null hypothesis (nh), which states, in physical terms, that projectile fragments are just ordinary nuclei, with no exceptional physical properties. We shall return to the quantitative formulation of this nh below.

The statistical problems that must be addressed in such a treatment of the data are the following:

(i) how to estimate a mean free path in a detector of finite dimensions (especially dimensions comparable to the mean free paths involved);

(ii) how to test the nh in the presence of a secondary "beam" with a wide charge spectrum. Indeed, since the mfp depends on the fragment's charge, the test must be carried out on subsamples characterized by individual charges; in any experiment with statistics comparable to ours, this necessarily implies subsamples of relatively small size;

(iii) assuming that an adequately constructed test has rejected the nh, how to extract from the data the pertinent information about the physical parameters characterizing the objects responsible for the anomaly.

This section deals with this set of problems. Fortunately, most of the statistical tests, estimators, and distribution laws involved in such a treatment turn out to be of the "text book" type and only a few variations on themes familiar from radioactive decay have had to be derived here. This section states definitions and results; details and/or proofs are given in subsections A–E of Appendix A.

Definition of the mean free path. The basic concept of this experiment is the reaction mean free path. If the target medium is homogeneous or if it has a length scale of inhomogeneity very small compared to the scale of the interaction distances,[14] the mean free path of a homogeneous particle beam appears as the parameter λ in the differential equation

$$\frac{dN_0}{dx}=\frac{-N_0}{\lambda} . \tag{4}$$

Here, N_0 is the number of particles incident on a target slab of thickness dx; some physical process, characterized by λ, removes particles from the beam. The solution of this equation is well known to be the negative exponential; specifically, the probability density for an interaction distance x is given by

$$f(x)=\frac{1}{\lambda}e^{-x/\lambda} . \tag{5}$$

Except for the fact that we are dealing with track lengths rather than with time intervals, this is just the law of radioactive decay, and many well-known results from this field (especially their application to the spontaneous decay in flight of unstable elementary particles) can be taken over to our analysis.

The probability density, Eq. (5), leads to several consequences. Foremost is the property that the negative exponential "has no memory." Physically, this means that any infinitesimal slab dx is equivalent to any other slab in which the particle may suffer an interaction, irrespective of the location of the slab. The fact that a particle has not interacted up to dx has no influence on its fate in dx.

Any given sample of tracks in a detector of finite length can be separated into two classes, viz., (i) those that did interact within the detector, and (ii) those that left the detector without interacting. One may choose to extract information on λ either by considering tracks of type (i) and (ii) *together* or by considering *only* the distribution of interaction distances of class (i).

A. Method *A*

The first method of estimation, which shall be denoted as method *A*, uses a moment of the interaction distance distribution *as well as* information about those tracks that did not interact. The second, which we shall denote as method *B*, will be dealt with in Sec. IV B.

The concept of method *A* can be formulated as follows:

(1) Assume λ is a constant.

(2) Follow tracks until N interactions are observed, $N \geq 1$.

(3) Sum the total path lengths followed for both the interacting and noninteracting tracks, where the path length of a particle's track is the length from its initial observation, i.e., either the scan line for beam particles or the location of the parent interaction for PF's, until its interaction point or its exit from the detector. Denote this sum by S_N.

(4) Define the estimate of the mfp as

$$\lambda^*=S_N/N . \tag{6}$$

1. *Distribution of the total path length in an infinite detector*

In order to establish that λ^* deviates significantly from some expected value λ, one would like to know the distribution law of λ^*, given λ and N. For practical reasons it is preferable to investigate instead the distribution law of the total path length S_N, given λ and N.

In an infinite detector, all tracks must interact; if the individual interaction length of the ith track is x_i, then by definition

$$S_N=\sum_{i=1}^{N} x_i \ .$$

Since the distribution of x_i, given λ, is known, Eq. (5), the probability density of S_N is obtained by N-fold convolution of Eq. (5) (see Appendix A, subsection A), which yields the Γ distribution[21]

$$f(S_N)dS_N=\frac{1}{\Gamma(N)}\left[\frac{S_N}{\lambda}\right]^{N-1} e^{-S_N/\lambda}\frac{dS_N}{\lambda} \ . \tag{7}$$

As any Γ distribution of (integer) order N can be transformed by a change of variable to a χ^2 distribution (see Appendix A, subsection B), it follows that the quantity

$$h^2\equiv\frac{2S_N}{\lambda} \tag{8}$$

is distributed like χ^2 with $2N$ degrees of freedom.

2. *Case of a finite detector*

Having established the distribution of S_N in an infinite detector, one can now apply it to the case of a finite detector. As long as there is an essentially unlimited number of tracks so that in any repeat experiment one can go to the Nth interaction, the distribution of S_N must be the same. To establish this fact, we invoke the no-memory property. Simply regard each track length in an infinite detector as being made up of noninteracting segments plus the last segment, which terminates in the Nth interaction. In an infinite detector, each track must interact, causing N to be identical to the number of tracks; in a finite detector, N is related to the flux N_0 by the binomial distribution at fixed flux, so that one in principle requires an arbitrary amount of flux to ensure that one reaches N in all cases. In fact, let T be the distance available for observation (i.e., the potential path) and $P_T=1-e^{-T/\lambda}$; then N is distributed binomially:

$$W(N)=\binom{N_0}{N}P_T^N(1-P_T)^{(N_0-N)} \ . \tag{9}$$

For $N_0\to\infty$ and N_0P_T finite, Eq. (9) tends toward a Poisson distribution and Eqs. (7) and (8) hold.

From the known properties of the χ^2 distribution,[22] it follows that the *relative* root mean square (rms) deviation of S_N and hence of λ^* at a given N is rigorously

$$\frac{\sigma(S_N)}{S_N}=\frac{\sigma_{\lambda^*}}{\lambda^*}=N^{-1/2} \ . \tag{10}$$

But, because the χ^2 distribution is only asymptotically normal (as $N\to\infty$) and quite skew at finite N, the rms deviation [Eq. (10)] should *not* be converted into "standard," i.e., Gaussian, confidence levels unless the sample size is very large. In practical terms this means that at a given λ, "upward" fluctuations, i.e., $\lambda^*>\lambda$, may be considerably more probable than "downward" ones.

A final remark: Because of the linear relationship between λ^* and S_N at fixed N, it follows that $\langle\lambda^*\rangle=\lambda$, i.e., λ^* is a consistent estimate for λ.

3. *Method A'*

Having established that the estimate $\lambda^*=S_N/N$ depends essentially only on the mfp λ and N, and is independent of detector size, one can subdivide a data sample and consider $\lambda^*(\eta)$, with η some variable on which λ has a known theoretical dependence. Likewise, using Eq. (3) one may construct $\Lambda^*(\eta)$. In particular, η may profitably be taken to be the distance after the point of first observation of a track as defined above; call this distance D. In this case it is clear that a constant λ (or Λ) is independent of D, and hence $\langle\lambda^*\rangle$ should also be independent of D. One may thus consider S_N and N binned in distance intervals $D_j\le D\le D_{j+1}$, which should give compatible results for λ^* irrespective of j. This method of examining $\lambda^*(D)$, and especially $\Lambda^*(D)$ (for a fixed value of b), will be termed method A'.

4. *Pooling information from PF's with different charges*

To increase statistics (especially in method A') one may choose to replace a set of λ_Z^* values, each

measured at a given Z, by the best estimate for Λ from this set.

As a consequence of the χ^2 distribution of h^2, Eq. (8), we use the method of maximum likelihood to estimate values of Λ and b in the power law approximation $\lambda=\Lambda Z^{-b}$ from a set of λ_Z^* measurements, say with N_z stars each. First, we take the logarithms of the probability density of the χ^2 distribution [Eq. (A14)]

$$\ln f=\ln(\tfrac{1}{2})-\ln\Gamma(N)+(N-1)\ln(N\lambda_Z^*) -N\ln\Lambda+Nb\ln Z-\frac{N\lambda_Z Z^b}{\Lambda} . \tag{11}$$

Equating the derivatives with respect to Λ and b to zero, and letting $S_z\equiv\lambda^*(Z)N_z$, one obtains Λ^*,b^* as solutions of the following system of equations:

$$\frac{\sum_Z S_Z Z^{b^*}}{\sum_Z N_Z}=\frac{\sum_Z S_Z Z^{b^*}\ln Z}{\sum_Z N_Z\ln Z} , \tag{12a}$$

$$\Lambda^*=\frac{\sum_Z S_Z Z^{b^*}}{\sum_Z N_Z} . \tag{12b}$$

5. *Comparison of two estimated mfp's*

In practice one is often confronted with the necessity of comparing two values of λ^*, say λ_1^* and λ_2^*, supposedly pertaining to measurements of the same physical process. This situation occurs either when one deals with two independent measurements or when one wishes to compare values of λ^* under different physical conditions, which may be assumed to have *no influence* on the value of λ. Let λ_1 and λ_2 be the expectation values of λ_1^* and λ_2^*, respectively. The nh to be tested is then

$$\lambda_1=\lambda_2\equiv\lambda . \tag{13}$$

It turns out that a convenient test quantity for this nh is the ratio

$$F\equiv\frac{\lambda_1^*}{\lambda_2^*} . \tag{14}$$

As long as Eq. (13) is true, F obeys a well-known distribution law, the so-called F, or variance ratio, distribution (see subsection C of Appendix A), *irrespective of the concrete value of* λ, with $2N_1$ and $2N_2$ degrees of freedom (N_1 and N_2 are the sizes of the samples from which λ_1^* and λ_2^* were derived): The cumulative distribution function (CDF) of this distribution is

$$P_F\equiv P(<F) =\frac{N_1^{N_1}N_2^{N_2}}{B(N_1,N_2)}\int_0^F t^{N_1-1}(N_2+N_1 t)^{-(N_1+N_2)}dt , \tag{15}$$

where B is the beta function. P_F is tabulated, e.g., in Ref. 22, and has the general property of CDF's, namely that it is uniformly distributed between 0 and unity [or briefly P_F is distributed $U(0,1)$]. Hence, its expectation value is $\frac{1}{2}$ and its dispersion is $\sigma_u\equiv(12)^{-1/2}$. Consider a set of ν values of P_F that have been obtained from pairs of λ_1^* and λ_2^*, where it is only necessary that the nh, Eq. (13), be true *separately for each pair,* i.e., λ may vary from one pair to the next. Then one may build the sample mean of the P values

$$\bar{P}_F\equiv\frac{1}{\nu}\sum_{j=1}^{\nu}P_{F,i} . \tag{16}$$

For large ν (in practice for $\nu\gtrsim 10$) the quantity

$$y_P\equiv\frac{\bar{P}_F-\frac{1}{2}}{\sigma_u/\sqrt{\nu}} \tag{17}$$

is approximately a normal deviate of zero mean and unit variance. An exact way of testing the nh, Eq. (13), at finite ν will be given below.

6. *Comparison of many estimated mfp's*

Consider the case when a set of, say, ν values $\lambda_1^*,\lambda_2^*,\ldots,\lambda_\nu^*$ have been measured, with N_1, $N_2,\ldots,N_\nu$ stars. Further, let $\lambda_1,\lambda_2,\ldots,\lambda_\nu$ be the mfp's that we *expect* from physical considerations (a special case could be $\lambda_1=\lambda_2\cdots=\lambda_\nu\equiv\lambda$), which occurs, e.g., in method A'). A convenient test statistic can be constructed as follows: (1) Compute for each λ^* the CDF of the S_N distribution $P_{Si}(h^2\mid\lambda_i,N_i)$ [Eq. (A15)]. (2) Note that, because each P_{Si} is distributed $U(0,1)$, its logarithm is exponentially distributed and hence the quantity

$$g_i^2\equiv-2\ln P_{Si} \tag{18}$$

obeys a χ^2 distribution with two degrees of freedom. (3) Compute the sum

$$g^2\equiv\sum_{i=1}^{\nu}g_i^2 . \tag{19}$$

Because of the additivity of χ^2 variables, g^2 is itself χ^2 distributed with 2ν degrees of freedom and

can, hence, be used to test the consistency of the λ^* values with their expectations.

Incidentally, the same statistical test can be used to pool in an exact way the information from many pairs of $(\lambda_1^*,\lambda_2^*)$ values, Eqs. (14) and (15). One has just to replace the P_{Si} in Eq. (18) by the P_{Fi} values [Eq. (15)]; then g^2 tests the hypothesis that all $(\lambda_{1i}^*,\lambda_{2i}^*)$ pairs have the same expected λ_i.

B. Method *B*

Thus far the statistical analysis has been concerned with both interacting and noninteracting tracks. It is necessary to consider also the case when only interacting tracks are used, for the additional insight we gain into the nature of the effect and because certain types of information are simply not available in any other way. To illustrate the first reason, we remind one that if the nh is true, methods *A* and *B* must yield consistent estimates for λ, irrespective of detector geometry. If, however, the nh must be rejected, methods *A* and *B* become dependent on the relative geometry of the detector, and of the events, and their results will disagree by amounts that depend on the abundance and properties of the objects responsible for the anomaly.

On the other hand, if, for example, one wishes to compare some statistic concerning the mfp for events tagged by a characteristic of their interaction star (like, among others, its multiplicity), the information can be derived from samples of *interacting tracks* only.

1. *The r-link chain topology*

Let us begin with the simplest case, the observation of a single interacting track. If the nh is true, there is a known single mfp λ. One measures two quantities, the interaction distance, X, and the potential path, T, which is the maximum distance over which the individual track could have been observed within the stack. (T is practically the same for all beam tracks and changes with each individual track for PF's.) Starting from Eq. (5), we obtain the probability density for X at a given potential path T (Ref. 21)

$$f_1(X)=\frac{(1/\lambda)e^{-X/\lambda}}{1-e^{-T/\lambda}}\ , \tag{20}$$

the CDF of which,

$$P_1(X)=\frac{1-e^{-X/\lambda}}{1-e^{-T/\lambda}}\ , \tag{21}$$

is distributed $U(0,1)$. Equations (20) and (21) are useful in two ways, viz.,

(i) the CDF P_1 can be used to test the nh. From a large number N of P_{1i} values one either tests whether $\bar{P}_1$ is consistent with $\frac{1}{2}$ or one computes g^2, Eq. (19), and performs the χ^2 test.

(ii) the product of N probability densities, Eq. (20), is used to construct the logarithmic likelihood

$$L=-N\left[\frac{\bar{X}}{\lambda}+\ln\lambda+\ln(1-e^{-T/\lambda})\right]\ , \tag{22}$$

where

$$\bar{X}=(1/N)\sum_{i=1}^{N}X_i\ .$$

The maximum likelihood estimate for λ is therefore the solution of the transcendental equation

$$\lambda^*=\bar{X}+\frac{T}{e^{T/\lambda}-1}\ . \tag{23}$$

The width of the likelihood curve and implicitly the error assigned to λ^* are functions of N *and* T/λ and increase rapidly as T/λ approaches unity.[21] For $T/\lambda \gg 1$, Eq. (23) turns into Eq. (6) with the error given by Eq. (10).

If each event has a different T value, Eqs. (22) and (23) are easily generalized; see, e.g., Ref. 21. We shall refer to all the above results as the one-link case.

However, the single track is not the only topology with which one must deal. Another common topology is the r-link chain. This is the topology when one has r ($r \geq 1$) PF collisions in a row. Consider the most frequently encountered case of $r=2$ on which we have concentrated here, i.e., the *two-link chain topology.* This topology is illustrated in Fig. 2, which is a microprojection drawing of a 1.88*A* GeV ^{56}Fe interaction (star) that leads to a two-link chain, where the secondary PF, with mfp λ_X, interacts after a distance X from the vertex of the primary ^{56}Fe interaction, and the tertiary, with mfp λ_Y, interacts after a distance Y from the vertex of the interaction of the secondary PF. The sum of the path lengths of the PF's $S=X+Y$ is indicated, as is T, the potential path length available for the secondary PF for interacting in the emulsion stack.

There are several different probability distributions one may construct from the X and Y in a two-link topology given the mfp's and T. One is $P_2(X)$, another $P_2(Y)$, which uses the X and Y in-

formation from each link *separately*. On the other hand, one may combine all the information into one variable, $S=X+Y$, the total length of the two-link event chain, and consider $P_2(S \mid T,\lambda_X,\lambda_Y)$ and the likelihood derived from this CDF. Since the charges Z_X,Z_Y are what one actually measures, and one then assumes

$$\lambda_X=\Lambda Z_X^{-b}\ ,\quad \lambda_Y=\Lambda Z_Y^{-b}\ ,$$

one may write

$$P_2(S \mid T,Z_X,Z_Y,\Lambda,b)$$

and examine the likelihood as a function of one parameter, e.g., Λ.

By solving the pertinent differential equations (subsection E in Appendix A), the CDF's for X, Y, and S can be written in the general form

$$P_{2\mu}=\frac{\pi_\mu(\mu)}{\pi_\mu(T_\mu)}\ , \tag{24}$$

where μ is either X, Y, or S,

$$T_X=T_S\equiv T,\quad T_Y=T-X\ , \tag{25}$$

and the functions π_μ are the following:

$$\begin{aligned}\pi_X&=1-e^{-X/\lambda_X}-(1-\rho)e^{-(T/\lambda_X)(\rho/\rho-1)}[1-e^{-X/(1-\rho)\lambda_X}]\ ,\ \text{if } \lambda_X\neq\lambda_Y\\ &=1-e^{-X/\lambda}\left[1+\frac{X}{\lambda}\right]\ ,\ \text{if } \lambda_X=\lambda_Y\equiv\lambda\end{aligned} \tag{26}$$

$$\pi_Y=1-e^{-Y/\lambda_Y}\ ,\ \text{in both cases} \tag{27}$$

and

$$\begin{aligned}\pi_S&=1-[\rho e^{-S/X}-(1-\rho)e^{-(S/\lambda_X)(\rho/\rho-1)}]\ ,\ \text{if } \lambda_X\neq\lambda_Y\\ &=1-\left[1+\frac{S}{\lambda}\right]e^{-S/\lambda}\ ,\ \text{if } \lambda_X=\lambda_Y\equiv\lambda\ ,\end{aligned} \tag{28}$$

with

$$\rho=\frac{\lambda_X}{\lambda_X-\lambda_Y}\ . \tag{29}$$

Note that all $P_{2\mu}$ are distributed $U(0,1)$ if the nh is true and all the pertinent tests, especially the reduction to a χ^2 distribution, Eq. (19), apply implicitly. Furthermore, it is noteworthy that $P_2(X)$ and $P_2(Y)$ are statistically independent; hence, a scatter plot of $P_2(X)$ vs $P_2(Y)$ should uniformly populate the unit plane. One simple test for uniformity is to divide this unit plane into quadrants by the lines $P_2(X)=\frac{1}{2}$, $P_2(Y)=\frac{1}{2}$ and test all possible asymmetries between any two quadrant populations M_{ij} or of linear combinations thereof.

Assigning indices 1 and 2 to events with $P_{2\mu}\leq\frac{1}{2}$ and $>\frac{1}{2}$, respectively, one can test for deviations from zero of such asymmetry coefficients as, e.g.,

$$C\equiv(M_{11}-M_{22})/(M_{12}+M_{21})\ . \tag{30}$$

Equation (30) will be applied to the data obtained via method B in Sec. V B, to test $P_2(X)$ and $P_2(Y)$ for statistical independence. The confidence levels assigned to C come from the multinomial distribution of the M_{ij}.

Finally, let us consider a situation in which the nh has been rejected by any or by all the tests mentioned hereto. If one is able to construct an alternate hypothesis, it is necessary to establish procedures for investigating its parameters. More specifically, if one makes the simplest alternate hypothesis (hereafter denoted by H_1) that only one sort of quasistable (over at least a few cm of flight path) anomalous projectile fragments (APF's) (Ref. 23) are responsible for the effect, we are interested in their relative abundance and their (assumedly unique) mfp λ_a.

Most events are obviously individual interacting PF's, which are one-link chains. Hence, one needs to use a modified one-link formula to obtain P values and likelihood functions. Assuming each track has a probability α of being an APF with a mpf λ_a, Eq. (21) can be generalized to

$$P_1(X \mid T,\lambda_Z,\alpha,\lambda_a)=\frac{(1-\alpha)(1-e^{-X/\lambda_Z})+\alpha(1-e^{-X/\lambda_a})}{(1-\alpha)(1-e^{-T/\lambda_Z})+\alpha(1-e^{-T/\lambda_a})}\ . \tag{31}$$

Differentiating Eq. (31), it is straightforward to calculate the likelihood as the product of the densities

$$f(X)=\frac{(1-\alpha)\frac{1}{\lambda_Z}e^{-X/\lambda_Z}+\frac{1}{\lambda_a}e^{-X/\lambda_a}}{(1-\alpha)(1-e^{-T/\lambda_Z})+\alpha(1-e^{-T/\lambda_a})} \tag{32}$$

for each (X,T) pair given the charge Z of the track.

C. Monte Carlo simulations

All the analysis in this section has been restricted to "exact" statistics, exact in quotations because the results of the statistical treatment are exact under assumptions valid only in a somewhat idealized world. In all methods depending on the hypothesis $\lambda_Z=\Lambda Z^{-b}$, both this form and the assumption that the exponent b is the same for PF's as well as for VOS occupants is an idealization. The F test (independent of λ), with the ratios F grouped as to laboratory and measured charge, needs only an assumption of relative homogeneity. This is our most powerful tool. Furthermore, when applying method A, one typically constructs S_N not according to its rigorous definition (total path length up to, but not beyond, N stars) but including all the path length observed, including a track segment beyond the Nth star. Although this correction is negligible in large samples, it may conceivably matter in the much smaller samples collected, e.g., at fixed charge, especially in the third or later generations. Finally, in any concrete experiment the incident flux is really finite.

How should one test whether or not these idealizations have any physically significant effect on the results? One possibility is to attempt ever improved analytic approaches. Since the number of physical effects one wishes to include may grow, this would involve a growing complexity of the statistical methods without any necessary gain in physical understanding. Another possibility is to use the methods based on idealized assumptions and analyze the results of simulations (which incorporate violations of the idealizations) by these same methods. In this subsection, the latter approach is elected.

A Monte Carlo simulation computer program was written. The output of this program was a data set in the identical computer format as the actual data of the experiment and hence could be analyzed by the same programs that were used to obtain the results.

The basic component in the simulation is the generation of random interaction distances, assuming that these come from the negative exponential distribution. These distances will be called simulated interaction distances (SID). SID's clearly depend on mfp, and the whole point of the simulation is to select the mfp's (and topologies) from physical considerations.

Since we want to simulate something as close to the actual data set as possible, we used the primary interaction distances and topologies (i.e., secondary PF tracks) as actually observed. The interaction distances alone will not generate tertiary and later generations unless a topology is assigned at the interaction vertex of a PF. To do this, all topologies (actually observed in the experiment, e.g., $O\rightarrow B+Li$, $Ca\rightarrow O+C$, $Ca\rightarrow O+2Li$, etc.) were stored in the computer grouped according to the charge of the parent; given the charge of the interacting PF, a topology was selected at random. The topology PF$\rightarrow$no further PF's (all $Z<3$) was also allowed to occur at random with its measured frequency. Through these procedures, simulated events were generated.

A PF was deemed to have interacted whenever its SID was less than its available potential path. SID's were kept to machine accuracy but were written on the simulated data file rounded off as the original observations. Thus, any error induced by rounding was incorporated. The only remaining question is how to assign mfp's to individual tracks.

The known systematics were incorporated into the simulation by modifying the mfp's from model calculations. For each true Z, calculated mfp's from a realistic geometrical model were used,[17] not ΛZ^{-b}. For each true Z, a true mfp was assigned, incorporating isotopic noise; sometimes $Z=8$ was given the mfp of ^{16}O, sometimes ^{18}O, etc. To get the true Z from the observed Z (the charge on the data file), an error was selected from the observed Z-reproducibility distribution (Fig. 3) coupled with a systematic bias if so chosen. Thus, both charge misidentification and isotopic noise were included. In fact, to keep the calculation robust against small changes in A, the isotopic effects were even increased by a factor of 2. If, e.g., isotope (Z,A') was predicted to have a 3% change in mfp from the VOS occupant (Z,A), a factor of 6% was actually used.

Thus, many copies of the pseudodata were produced. Each copy was fed through the analysis program package and pseudoresults generated. We

briefly present the result of analyzing all these pseudodata put together, first for method *A* and then method *B*.

(1) Method A. We present in Fig. 5 the $P(F)$ distribution for Monte Carlo events grouped according to laboratory and charge and subjected to the same distance cut as the experimental data, viz., 2.5 cm. The mean and rms deviations of this distribution are $\bar{P}=0.50\pm0.02$ and $D_P=0.296\pm0.012$; both values are consistent within errors with the expected $\langle P\rangle=\frac{1}{2}$ and $D_P=\sigma_u$. Similarly, results for Λ^* were observed not to depend on either distance from the parent star or the generation of the PF, as expected if the nh were true.

(2) Method B. Here again, things are as expected under the nh. For illustration, we examined the distribution of $P_2(S)$ in the simulated two-link chains and the pertaining likelihood curve. We find $P_2(S)=0.50\pm0.02$; the likelihood curve averaged over 100 Monte Carlo repeats is displayed in Fig. 6. It peaks at $\Lambda^*=29.6$, with rms deviations as illustrated.

In all cases, a normal simulation, using conventional nuclear physics and the systematics of this experiment, produces normal physics in the sense that the numbers obtained from the simulation are practically indistinguishable from the values expected from the idealized model underlying our equations. Hence, we are compelled to conclude that the statistical methods presented in Secs. IV A and IV B are valid for a physical understanding of the data. The simulation gives results in contradiction with our observations, as will be shown in Sec. V.

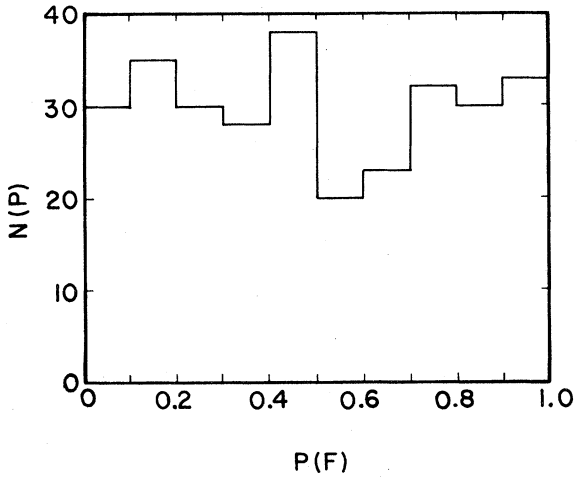

FIG. 5. Histogram of the distribution of probabilities $P(F)$ for Monte Carlo generated events grouped according to charge, laboratory, and subjected to the same $D\lesssim 2.5$ cm cut as the data.

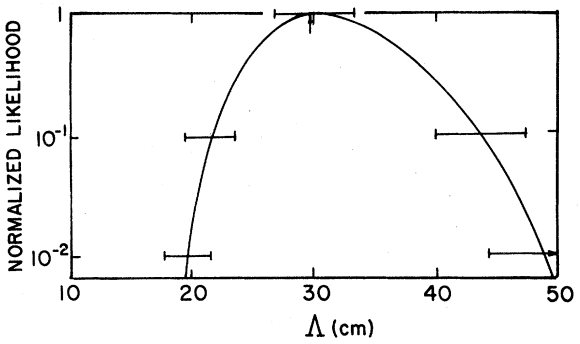

FIG. 6. The normalized likelihood curve for the parameter Λ, Eq. (3), based on repeated independent Monte Carlo simulated two-link chains. The error bars represent the observed deviations about the mean likelihood curve.

V. RESULTS

A. Overview

We now proceed to apply the methods of analysis described in Sec. IV to the results of our experiment. An overview of the tests applied to our data is given in Table II, which is also meant to illustrate why each of the tests was necessary.

The first half of this table shows the checks of our methods of analysis when applied to primary (i.e., normal) beams. Its second half deals with fragments emerging from the primary interactions. Here the different rows refer either to different subsets of the data or to different groupings of a given subset. We now discuss these tests in detail.

B. Method *A*

The first application of this method is presented in Fig. 7, where the mfp λ^* observed for primary ^{16}O beam nuclei is plotted as a function of the distance from the scan line (pickup point) of the incident beam. The data are well accounted for by a constant value of λ^*, the straight-line fit to the data at $\bar{\lambda}^*=11.9$ cm having a $\chi^2=7.3,12$ DOF (degrees of freedom) obtained through the procedure described in subsection D of Appendix A. The observation that λ^* does not depend on D is typical of the behavior of all mfp measurements of beam nuclei.

Figure 8 presents the mean-free-path parameter Λ^* of all secondary and later generation PF's, plot-

TABLE II. Overview of the different statistical tests applied to our data and of the motivation for their use. The table lists the quantities necessary to test both the normality of the accelerator beams and the abnormality of projectile fragments, using either interacting tracks *only* (method *B*) or interacting as well as noninteracting tracks (method *A*). The confidence levels express the probability that the result could have occurred as a statistical fluctuation assuming the null hypothesis (normality) to be true.

Particle	Method	Quantity measured	Statistic and/or its expected distribution	Parameters or constraints	Confidence level %	What does it show?
Beam	*A*	λ^* at different D	$2S_N/\lambda$ χ^2		11	Validity of method *A'*. λ^* does not depend on localization of segment. Uniform scanning efficiency.
		λ^*_{Di} vs λ^*_{Di+1}	$\lambda^*_{Di}/\lambda^*_{Di+1}$ F		69	Correct fluctuations of λ^* estimates.
	B	Distribution of interaction distances	Exponential	λ^*	22	Compatibility of methods *A* and *B*.
PF's	*A*	Λ^* for $D<2.5$ cm	$\simeq$ Gaussian	b_{beam}	0.04	Assuming parametrization ΛZ^{-b} mfp's near origin are shorter than those of beam nuclei.
		Λ^* for $D>2.5$ cm	$\simeq$ Gaussian	b_{beam}	34.5	Away from origin mfp's are compatible with beam values.
		λ^* at $D \gtrless 2.5$ cm	F	Fixed Z and laboratory	0.03	mfp is shorter near origin irrespective of parametrization and of calibration of beams.

TABLE II. (*Continued.*)

Particle	Method	Quantity measured	Statistic and/or its expected distribution	Parameters or constraints	Confidence level %	What does it show?
PF's	*A*	λ^* for secondary vs later generations	*F*	Fixed *Z* and laboratory	0.07	Later generations exhibit shorter mfp's than secondaries.
	B	Distribution of interaction distances	Sum of exponentials	Minimum *T*	0.03	Excess of stars near origin for a subset with controlled minimum potential length.
				as well as ↓		
		Lengths of one link chains	$P\ (<x)$ uniform	T Λ_{beam} b_{beam}	0.002	Too short interaction lengths irrespective of potential length.
		Lengths of 1st and 2nd link in two link chains	Scatter plot $P\ (<y)$ vs $P\ (<X)$ uniform		0.1	Short secondaries give rise preferentially to short tertiaries (memory).

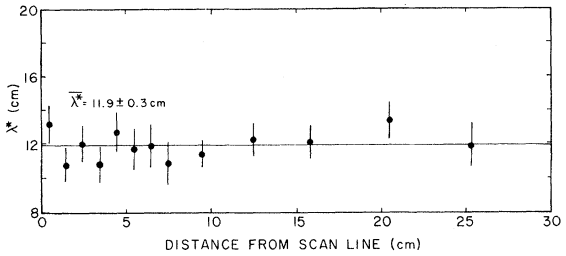

FIG. 7. Measurements of the primary 2.1*A* GeV ^{16}O mfp as a function of the distance from the scan line.

ted as a function of distance D from the origin of emission of the PF. The quantities Λ^* are calculated under the assumption that $\lambda=\Lambda Z^{-b}$ with $b=0.44$ for the LBL data and $b=0.43$ for the NRC data. For simplicity of display, we have renormalized all data using a constant mean value of $\Lambda_{\text{beam}}=30.4$. The error bars we have assigned to the data points represent one standard deviation *assuming the primary beam value for* Λ. Thus, for example, if $\Lambda^*=20$ cm with 100 stars and $\Lambda_{\text{beam}}=30$ cm, then (in the approximation to which $\sqrt{N}$ statistics apply) $\Lambda^*=20\pm3$ cm, *not* $\Lambda^*=20\pm2$ cm. This is because it is assumed at the outset that all PF's should have the mfp parameter Λ as measured on primary beams and that the Λ^* values are just fluctuations around this value.

In contrast to both expectation and observation on primary beams, the values for Λ^* are low for the first several centimeters; they become compatible with Λ_{beam} for distance $D\gtrsim5$ cm. The short mfp's at small distances D imply that there is an excess in the number of interactions at these distances.

This result can be visualized also by considering the frequency distributions of interaction distances $N(X)$. For clarity, we have performed the analysis at fixed potential path T_1. To fix T_1, we demanded that each track *could* have gone *at least* T_1 cm, even if it interacted within T. The $N(X)$ distributions for $T_1=3$ and 9 cm, summed over all PF's, are displayed as Fig. 9. Examine the $T_1=3$ cm result. Here, with a total of 2386 tracks, we expect 504 stars assuming for the mfp's the results of the fits to primary beams. In the data, there are actually 581 stars, a fluctuation expected to occur with a probability 3×10^{-4}. The curves in Fig. 9 are calculated assuming the same mixture of PF's as used in Fig. 8. They are obviously in good agreement with the data.

To obtain some insight as to the nature of this excess of interactions of PF's at short distances, we make the following simple assumption: In addition to PF's with normal mfp's, there is present another species of PF's, APF's, that are produced with probability α, having a constant, "anomalously short," mfp λ_a. We thereby assume that α and λ_a are independent of Z, which clearly may be an oversimplification of the physical situation. In this model the characteristic shape of the Λ^* vs D curve is due to the removal of APF's from the secondary beam by nuclear collisions so that at infinity the beam consists only of normal nuclei. By the procedure explained in Sec. IV B, we find that $\alpha^*\simeq0.06$ and $\lambda_a^*\simeq2.5$ cm. These results are illus-

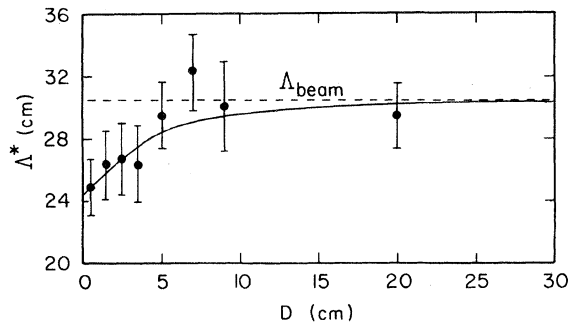

FIG. 8. Estimates Λ^* for the mfp parameter Λ at different distances D from the origins of the PF's: full circles, experiment; dashed line, prediction from Λ_{beam}; solid line, prediction assuming a 6% beam admixture of PF's with $\lambda_a=2.5$ cm.

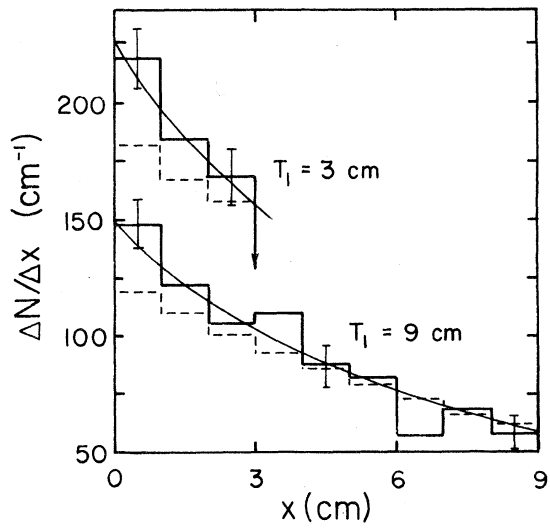

FIG. 9. Distribution of interaction distances x for events with potential paths $T\leq T_1$; dashed and solid lines have the same meaning as in Fig. 8.

trated in Fig. 10, where the normalized likelihood contours for the parameters α and λ_a are displayed for $0<\alpha<0.5$ and $0.1<\lambda_a<20$ cm. Although the maximum likelihood occurs at $\alpha=0.06$, $\lambda_a=2.5$ cm, the data are compatible with α and λ_a several times larger than the most likely values deduced from this elementary model.

The smooth curves in Figs. 8 and 9 are calculated assuming this model. In terms of the expectation values of all variables, the value of $\langle\Lambda\rangle$ in the jth interval (from D_j to D_{j+1}) is then

$$\langle\Lambda\rangle_j=\frac{\sum_Z \phi_{Z,j}[(1-\alpha)p_{Z,j}\lambda_Z+\alpha p_{a,j}\lambda_a]Z^b}{\sum_Z \phi_{Z,j}[(1-\alpha)p_{Z,j}+\alpha p_{a,j}]}\ , \tag{33}$$

where $\phi_{Z,j}$ is the number of tracks of charge Z, incident on segment j,

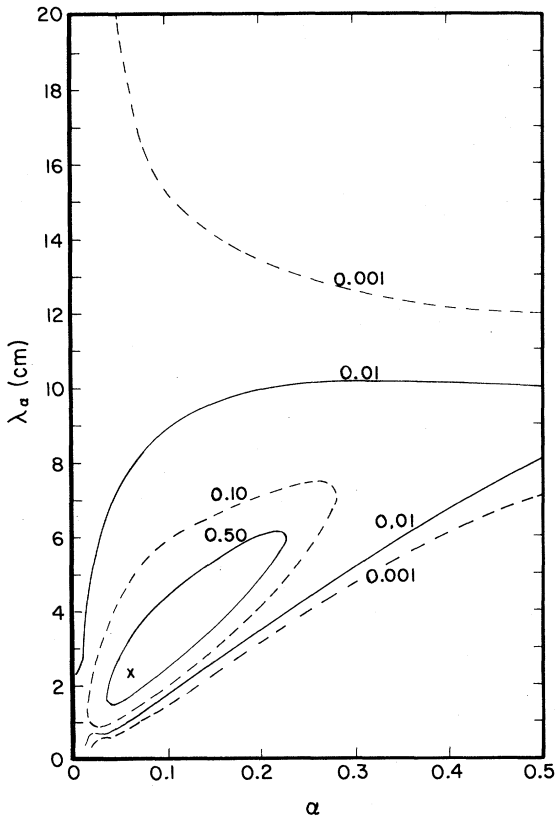

FIG. 10. Normalized likelihood contours for the parameters λ_a and α, Eq. (32), from all 1460 one-link chains. The cross indicates the position of the maximum likelihood.

$$\begin{aligned}\lambda_Z&=\Lambda_{\text{beam}}Z^{-b}\ ,\\ p_{Z,j}&=e^{-D_j/\lambda_Z}-e^{-D_{j+1}/\lambda_Z}\ ,\\ p_{a,j}&=e^{-D_j/\lambda_a}-e^{-D_{j+1}/\lambda_a}\ .\end{aligned} \tag{33'}$$

The calculated dependence of $\langle\Lambda\rangle$ on distance D agrees well with the observations. The reason the short mfp effect has been termed anomalous is clearly seen here. If one attempts to increase λ_a to, say, 10 cm, there is no value of α that will reproduce the observations well. They seem to require the existence of a component of the PF's produced with a few percent probability, with mfp's outrageously shorter than any of the primary beams employed. A value of 10 cm is already ludicrous, considering that this implies a nucleus of charge in the calcium range among PF's from oxygen. A 2.5 cm component is probably a shorter mfp (i.e., a larger cross section) than that of uranium.

If the short mfp is due to the cooperative effect of a few baryons (a "damaged zone") bound to a normal nuclear fragment, one could understand the approximate independence of λ_a from charge.

Suppose that "λ" of the damaged zone were λ_W; then

$$\lambda_a\approx(1/\lambda_W+1/\lambda_Z)^{-1}\ . \tag{34}$$

If we take $\lambda_W=3.5$ cm, for example, and $\lambda_{Z=26}=7$ cm, then $\lambda_a\simeq 2.3$ cm; on the other hand, for $\lambda_{Z=3}=18$ cm and the same λ_W, $\lambda_a\approx 2.9$ cm. Thus, for nuclides from Fe to Li, the equivalent APF mfp λ_a would change only from 2.3 cm to 2.9 cm, a difference that is undetectable with the present statistical accuracy of data. While the assumption of a damaged zone and of one anomalous component is probably too crude in every detail, it does reproduce the overall observations.

We now ask the question: Is the appearance of the anomalously short mean free paths for PF's an artifact caused by the use in our analysis of the power law fit, Eq. (3), and/or by the intermixing of data from the ^{16}O and ^{56}Fe experiments? To address this question we shall examine separately the mfp data from each laboratory at a fixed fragment charge Z. Each group of data was then subdivided into two subgroups: (i) $D\leq 2.5$ cm, yielding λ_1^*, with N_1 stars and (ii) $D>2.5$ cm, yielding λ_2^*, with N_2 stars. We thus obtain a pair of λ^* values for each charge Z, labeled by NRC or LBL, evaluated for distances $D\lesssim 2.5$ cm. The distance 2.5 cm is taken to be equal to λ_a^*, the mfp of the APF component given by the previously described maximum likelihood fit to the data.

For each pair of λ^* values take the ratio $F=\lambda_1^*/\lambda_2^*$. Given the number of stars N_1 and N_2, we compute the probabilities P_F for the measured ratios F under the assumption that λ_1^* and λ_2^* are from the same population [Sec. IV, Eq. (15)]. The individual mfp values recorded for each charge, separately for each primary beam, are shown in Table III along with the raw data from which they were derived. The CDF values $P\ (<\chi^2)$, which test the compatibility of the observed mfp's with those predicted from Eq. (3), and with measurements on primary beams, are given for illustration purposes only, since Eq. (3) is known to be only approximately valid. The weight of the argument rests on the last two columns, which give F and $P(F)$ for each individual charge and are hence free of the above-mentioned approximations. The histogram of the resulting $P(F)$ values is shown in Fig. 11(a). Recall that if the values of λ_1^* and λ_2^* were from the same population, the probabilities P must be distributed $U(0,1)$. The cross-hatched area represents the six charges from NRC, and the remaining area the 24 charges from LBL. It is immediately visible that the observed distribution has an excess of low P

TABLE III. Detailed experimental information used in the F test for the comparison of estimated mean free paths at small and at large distances D from the origin of the projectile fragments. For each primary beam and for each fragment charge the table lists the numbers of tracks incident on the segment under consideration, the number of interactions occurring in the segment, the estimated mean free path, and the cumulative probability for this value to occur as a fluctuation assuming the null hypothesis as well as the parametrization $\lambda_Z=\Lambda Z^{-b}$ to be valid. The last two columns give the value of the ratio F of the two estimates as well as the cumulative probability for F to lie below the observed value (without any assumption about the parametrization of λ_Z).

Laboratory and beam	PF charge	$D\leq 2.5$ cm				$D>2.5$ cm					
	Z	Tracks	Stars	λ_Z^*	$P\ (<\chi^2)$	Tracks	Stars	λ_Z^*	$P\ (<\chi^2)$	F	$P\ (<F)$
NRC	3	148	27	12.6	0.040	119	79	13.2	0.004	0.960	0.443
	4	93	23	8.7	0.004	69	46	13.9	0.172	0.623	0.039
	5	157	28	12.6	0.236	127	78	14.8	0.535	0.853	0.250
^{16}O	6	278	50	12.6	0.320	227	144	15.3	0.936	0.823	0.127
	7	193	40	10.7	0.162	150	110	10.9	0.072	0.978	0.463
	8	133	29	9.9	0.185	103	71	11.6	0.401	0.860	0.261
LBL	3	116	18	14.5	0.132	89	20	22.7	0.783	0.637	0.087
	4	123	21	13.1	0.131	95	32	13.8	0.130	0.946	0.429
	5	128	18	15.8	0.556	105	32	15.0	0.433	1.056	0.584
	6	139	20	15.8	0.689	111	31	16.5	0.801	0.955	0.445
	7	119	20	13.1	0.485	90	24	16.5	0.864	0.796	0.230
	8	109	18	13.4	0.620	83	27	15.0	0.829	0.893	0.364
	9	72	26	5.5	0.0002	45	17	14.0	0.764	0.388	0.001
	10	76	13	12.9	0.689	59	14	18.7	0.980	0.687	0.170
	11	64	15	9.5	0.312	47	12	18.3	0.977	0.520	0.045
	12	69	21	6.7	0.029	45	18	9.9	0.409	0.678	0.113
^{56}Fe	13	64	11	12.9	0.812	50	19	9.0	0.312	1.435	0.839
	14	55	17	6.3	0.049	35	14	10.6	0.632	0.594	0.074
	15	42	8	11.5	0.737	32	17	7.6	0.196	1.512	0.848
	16	58	17	7.2	0.164	40	21	8.5	0.345	0.848	0.313
	17	44	10	9.6	0.596	33	15	9.0	0.513	1.059	0.566
	18	38	11	7.2	0.280	26	14	7.0	0.210	1.037	0.542
	19	25	6	8.6	0.534	19	12	5.6	0.090	1.532	0.820
	20	27	9	6.4	0.236	18	5	20.4	0.992	0.313	0.016
	21	30	9	6.4	0.261	20	9	10.3	0.779	0.623	0.162
	22	30	8	8.4	0.582	21	8	11.9	0.893	0.709	0.250
	23	20	8	5.1	0.140	12	8	5.6	0.199	0.910	0.426
	24	26	12	3.9	0.017	13	11	5.3	0.124	0.734	0.229
	25	20	11	3.4	0.010	9	8	3.2	0.021	1.042	0.525
	26	20	10	3.2	0.011	10	6	7.5	0.546	0.423	0.043

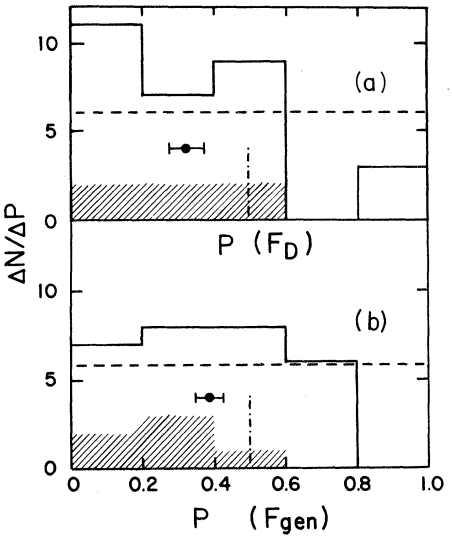

FIG. 11. Experimental frequency distribution of $P(F)$: (a) F_D, comparison by distance from the emission point; (b) F_{gen}, comparison by generation. The dashed line is the expected $U(0,1)$ distribution. The points with error bars are the experimental means $\bar{P}$, to be compared to their expectation $\langle P\rangle=\frac{1}{2}$. The shaded area refers to the results from NRC. Compare with Monte Carlo result from the nh shown in Fig. 5.

values; the values of P have been calculated such that this corresponds to $\lambda_1^*<\lambda_2^*$. As a statistic, the mean probability $\bar{P}$, Eq. (16), has the value 0.323, calculated from the unbinned P values. Here and hereafter deviations of any P value from its expectation $P=\frac{1}{2}$ will be expressed through the value y_P, Eq. (17), i.e., in terms of equivalent standard deviations along with the corresponding one-sided probabilities for such a deviation to occur as a random fluctuation. In the present case $y_P=-3.4$, a deviation expected to be exceeded by fluctuations about three times in 10^4 trials.

In other words, there are fewer than three chances in 10^4 that the λ_1^* values, taken charge by charge and laboratory by laboratory, come from the same population as the λ_2^* values. We therefore conclude that the mfp's of PF's are significantly shorter at small distances (i.e., $D<2.5$ cm) from their points of emission, than at greater distances, and that the low values of Λ^* at short D are not an artifact. More important for its physical implications, this result is independent of many systematic problems that potentially plague other methods. It only assumes relative homogeneity of the mfp's of the PF's at fixed Z. Traditional isotopic effects should by no means cause such an observation. Thus, we are compelled to conclude that there is something abnormal about the mfp's of PF's within the first few cm after their emission.

In addition to a comparison of λ^* at different distances after emission, one can also compare the mfp's of PF's from different generations. Primary beam nuclei do not have a short mfp component, while their progeny seem to evidence one. Is this effect independent of generation (starting with the second) or does it change with different PF generations? For example, as soon as APF's are assumed to be present, the use of method A for estimating λ fails in the sense that its results are no longer independent of detector geometry. The reason for this failure is that the relative population of APF's among *interacting* tracks increases as the potential path decreases. Because the potential paths decrease, on the average, with increasing generations (which occur at increasing depths in the target), it follows that, even without any further effects, shorter overall mfp's or PF's in the later generations are to be expected. It is also evident that if some conserved quantity is associated with the APF's (e.g., a damaged zone), the anomaly might persist through more than one generation, further decreasing the average mfp in later generations.

To test whether the mfp's change from generation to generation, we shall compare the mfp's of secondary PF's with those of tertiary and later generation PF's. Following the same procedure as above we compute

$$F_{\text{gen}}=\lambda_{\text{III}}^*/\lambda_{\text{II}}^* . \tag{14'}$$

The F_{gen} values, recorded separately for each PF charge and each primary beam, are given in Table IV along with the raw data from which they were derived (the structure of Table IV is otherwise identical to that of Table III). The histogram of the values of $P(F_{\text{gen}})$ is given in Fig. 11(b). There are six charges from NRC and 23 from LBL (there were not enough tertiary tracks of $Z=21$ to obtain any interactions). The one SD confidence interval about $\langle P\rangle=\frac{1}{2}$ is $\pm\sigma_u(29)^{-1/2}$; the observed mean is $\bar{P}=0.387$, which has $y_P=-2.11$, Eq. (17). However, we note that the highest P value recorded is 0.778. The probability to observe zero events in the uniform distribution, out of 29 attempts, with the binomial distribution parameter $p=0.778$, is 7×10^{-4}. Hence, the mere absence of any value of $P(F_{\text{gen}})>0.778$ is unusual, as one would expect about six counts in this interval.

This also appears to some extent in the values of Λ^* for different generations. Secondaries have

TABLE IV. Detailed experimental information used in the F test for the comparison of estimated mean free paths in the second and in later generation of projectile fragments. Except for the definition of F, the variables displayed are the same as in Table III.

Laboratory and beam	PF charge	Secondaries				Third and later generations					
NRC	Z	Tracks	Stars	λ_Z^*	$P(<\chi^2)$	Tracks	Stars	λ_Z^*	$P(<\chi^2)$	F	$P(<F)$
	3	117	87	13.3	0.003	31	19	11.7	0.042	0.880	0.329
	4	64	51	12.4	0.042	29	18	11.4	0.093	0.916	0.392
	5	104	73	15.2	0.645	53	33	11.8	0.129	0.775	0.122
^{16}O	6	228	158	15.3	0.949	50	36	11.3	0.165	0.740	0.062
	7	178	140	11.0	0.062	15	10	8.4	0.133	0.758	0.237
	8	128	96	11.2	0.284	5	4	7.6	0.249	0.673	0.285
	3	82	27	20.7	0.647	34	11	14.3	0.192	0.692	0.172
	4	87	41	14.1	0.124	36	12	11.5	0.113	0.811	0.287
	5	95	40	15.4	0.482	33	10	15.0	0.492	0.975	0.500
	6	98	41	15.4	0.689	41	10	19.6	0.871	1.272	0.778
LBL	7	79	34	14.8	0.731	40	10	15.6	0.716	1.051	0.580
	8	74	33	15.0	0.845	35	12	12.7	0.542	0.852	0.340
	9	57	36	9.1	0.057	15	7	7.7	0.164	0.849	0.385
	10	49	18	16.3	0.950	27	9	15.0	0.827	0.921	0.440
	11	44	17	16.7	0.972	20	10	7.7	0.167	0.461	0.035
	12	51	30	8.4	0.115	18	9	7.5	0.190	0.895	0.414
^{56}Fe	13	51	25	10.2	0.512	13	5	11.6	0.664	1.136	0.645
	14	41	24	8.4	0.221	14	7	8.0	0.332	0.956	0.490
	15	35	22	9.1	0.425	7	3	7.0	0.371	0.768	0.401
	16	53	36	8.0	0.182	5	2	6.5	0.405	0.820	0.484
	17	34	21	8.9	0.480	10	4	11.0	0.705	1.232	0.695
	18	31	20	7.8	0.295	7	5	4.3	0.097	0.555	0.160
	19	22	16	6.8	0.193	3	2	4.7	0.289	0.683	0.391
	20	23	10	15.2	0.983	4	4	1.8	0.011	0.120	0.002
	21	27	18	7.7	0.456	3	0				
	22	23	13	10.0	0.797	7	3	11.0	0.767	1.103	0.613
	23	17	14	5.2	0.073	3	2	6.7	0.494	1.293	0.703
	24	25	22	4.5	0.010	1	1	5.3	0.492	1.191	0.686
	25	19	18	3.4	0.001	1	1	2.1	0.240	0.629	0.461
	26	19	15	5.1	0.085	1	1	0.8	0.097	0.153	0.141

$\Lambda_{II}^*=28.8$ cm, 1196 stars, while later generations have $\Lambda_{III}^*=25.2$ cm, 264 stars. This has a probability of about 0.03 to occur. At face value, $\Lambda_{III}^* < \Lambda_{II}^*$, a result that is indicative of a larger admixture of APF's in later generations. We shall return to this topic in subsection V B.

Another technique we have used to examine the mfp data is to pool them within charge bins $3 \leq Z \leq 8$ (where PF's from both ^{16}O and ^{56}Fe primaries contribute), $9 \leq Z \leq 16$, and $17 \leq Z \leq 26$ (where only PF's from ^{56}Fe contribute), and to evaluate λ_1^* and λ_2^* without use of the length-weighting factor Z^b. The results are tabulated in Table V. For comparison, the prediction from $\lambda_Z = 30.4 Z^{-0.44}$ cm, weighted by the actual distri-

TABLE V. Estimates for the charge averaged mean free path λ and for the parameter Λ at different distances D from the origins of PF's for grouped charges. Expected values assuming Eq. (3) are given in the last column.

Z	$\bar{\lambda}^*$ ($D \leq 2.5$ cm) (cm)	$\bar{\lambda}^*$ ($D > 2.5$ cm) (cm)	$\langle\lambda\rangle$ (cm)
3–8	12.4±0.7	14.0±0.5	14.6
9–16	8.3±0.7	11.6±1.0	10.6
17–26	6.0±0.6	8.0±0.8	8.4
	Λ^* ($D \leq 2.5$ cm) (cm)	Λ^* ($D > 2.5$ cm) (cm)	$\langle\Lambda\rangle$ (cm)
3–26	25.0±1.1	30.0±1.0	30.4

bution of charges in each bin, is presented, this being the average fit to both NRC and LBL primary VOS beam data. The pooling was done by summing the total path length observed within the appropriate distance and charge intervals and dividing this by the number of stars. Again, inspection of the data in Table V reveals that within 2.5 cm of emission, PF's have short mfp's, while at longer distances, primary beam expectations are essentially fulfilled. The values of Λ^* for $D \lesssim 2.5$ cm, assuming $\lambda_z = \Lambda Z^{-0.44}$, are also listed in Table V. These estimates are 3.3 standard deviations apart, having a probability P_F, Eq. (15), of 5×10^{-4}.

C. Method *B*

After having observed by means of method *A* an apparent shortening of Λ^* in the first several cm, we now turn our attention to method *B* in order to extract the specific information inherent to those PF's that interacted.

First we consider all one-link chains. There are 1460 PF induced stars in these chains, and assuming that λ_Z has the values predicted by the LBL and NRC fits to primary VOS beams, we obtain the $P_1(X)$ histogram shown in Fig. 12. The mean of the distribution is

$$\bar{P}_1 = 0.469 \pm \sigma_u (1460)^{-1/2} .$$

This corresponds to $y_P = -4.1$ or to a probability of 2×10^{-5}.

The logarithmic likelihood curve of these data is displayed in Fig. 13; the peak is at $\hat{\Lambda} = 22.8$ cm.[24] The primary beam value is down three orders of magnitude on the likelihood curve. Furthermore, the same data within the context of method *A* (which includes noninteracting tracks) yield $\Lambda^* = 28.2$ cm, a value that is down by two orders of magnitude on the likelihood curve. Thus, $\hat{\Lambda} < \Lambda^*$. However, as stressed in Sec. IV, the method *A* and method *B* estimates must be consistent if the nh is true. One case for which this is expected, and found to be patently true, is demonstrated in Fig. 14, where the NRC primary ^{16}O, method *B*, likelihood curve and the method *A* result are displayed.

We now turn to two-link chains (Fig. 2), which offer us the opportunity to study correlations between successive generations of PF's. For $Z \geq 3$, there are 215 secondary-tertiary chains. In fact, there are 222 cases of tertiary stars, which means there are a few "forks." In the case of forktype events, we arbitrarily selected one of the branches at random, thus converting a fork topology to chain topology.

Consider Fig. 15, which presents the likelihood curves for Λ given the observed X, Y, and $S = X + Y$ measurements for each event. As demonstrated here, secondaries that gave a tertiary that interacted have $\hat{\Lambda}_X = 21.8$ cm, tertiaries have $\hat{\Lambda}_Y = 18.2$ cm, and the total length of the chain S has $\hat{\Lambda}_S = 19.8$ cm. Once the nh is rejected by the results of the preceding paragraphs, the inequality $\hat{\Lambda}_Y < \hat{\Lambda}_X$ could be qualitatively predicted by assuming a constant probability for emission of APF's in all generations. Indeed, as already stated, the stars

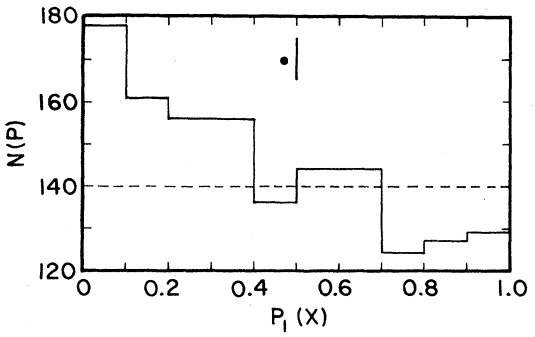

FIG. 12. The experimental frequency distribution of $P_1(X)$, Eq. (21). The histogram is the data. The solid vertical line is the expected value for the mean $\langle P \rangle = \frac{1}{2}$, while the solid circle is the observed value of $\bar{P}$; the error bars on $\bar{P}$ are the size of the solid circle. The dashed line is the expected $U(0,1)$ distribution. Note that the ordinate starts at 120 and that the $U(0,1)$ distribution is normalized *not* to the data but to the nh.

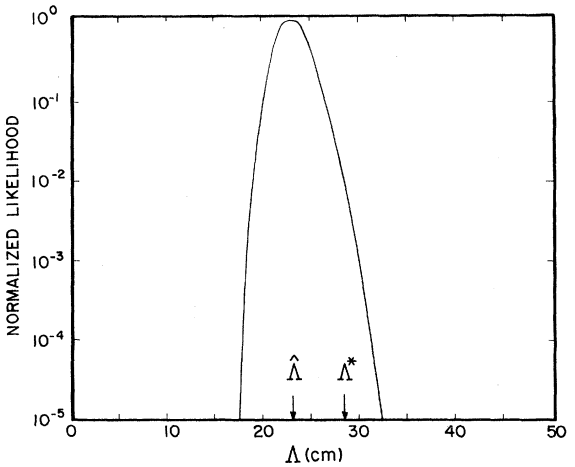

FIG. 13. The normalized likelihood curve for the parameter Λ based on the same data as in Fig. 12. The maximum likelihood value is $\hat{\Lambda} = 22.8$ cm; the method *A* estimate is $\Lambda^* = 28.2$ cm.

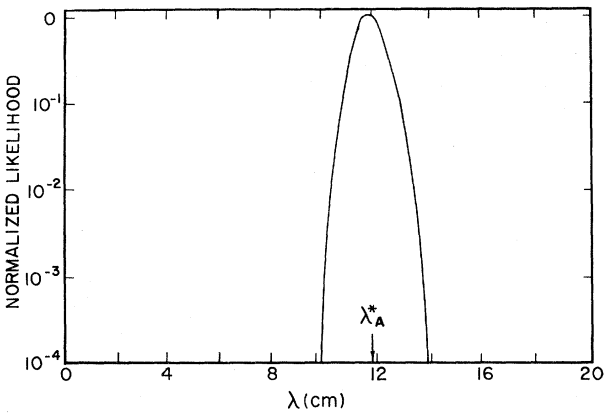

FIG. 14. The normalized likelihood curve for the parameter λ from the NRC primary ^{16}O data treated as one-link chains. The value of the method A estimator, $\lambda^*_A = 11.9$ cm, is shown and is equal to the position of the maximum value of the likelihood curve.

in the third and later generations are more heavily "infested" by APF's because of their shorter average potential paths. However, if one plots $P_2(X)$ against $P_2(Y)$, i.e., if one looks for possible correlations between the links in two-link chains, an interesting observation emerges.

As they have been defined in Sec. IV, the quantities $P_2(X)$ and $P_2(Y)$ are independent and each should obey a uniform distribution from 0 to 1 if

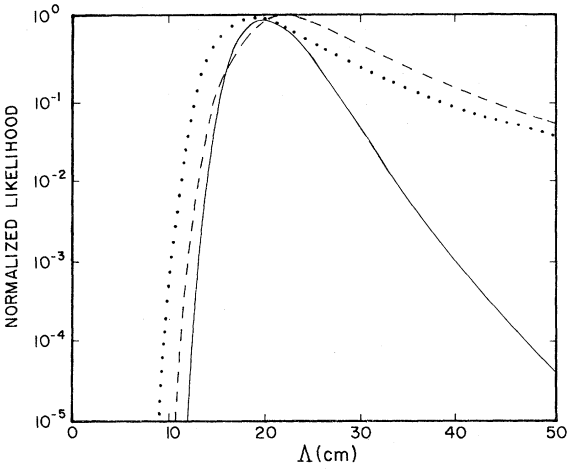

FIG. 15. The normalized likelihood curves for the parameter Λ from the experimental X, Y, and S of two-link chains. The dashed line is the result from the X distribution, the dotted line is the result from the Y distribution, and the solid line is the S distribution [compare to Fig. 6, where the (S distribution) Monte Carlo simulation likelihood curve is displayed]. The curves have been slightly displaced vertically at the peak for clarity.

the nh is true; hence, a scatter path of $P_2(X)$ vs $P_2(Y)$ should uniformly populate the unit plane. The result is shown in Table VI, where we have binned the data in two intervals of P, viz., 0 to $\frac{1}{2}$ and $\frac{1}{2}$ to 1, on both axes. The asymmetry coefficient C, Eq. (30), has the value

$$(75-46)/(47+47)=0.3\ ;$$

this is to be compared with the expectation $\langle C\rangle = 0\pm 0.1$. In terms of probability, the observed value deviates by 3 SD's (standard deviations) from its expectation.

We demonstrate in Table VI that a low value of $P_2(X)$ gives rise to a low value of $P_2(Y)$. Because a low P value corresponds to a short interaction distance (corrected for potential path), it follows that this result can be interpreted as a clear hint of "memory," by which we mean a "short" PF parent gives rise on the average to a short PF progeny. This property of memory would follow naturally if conserved quantum numbers are involved in the interactions of the hypothetical APF's. Further implications of the numbers in Table VI are discussed in Appendix C.

VI. DISCUSSION OF RESULTS

A. Statistical fluctuations

The first objection to the reality of the effects discussed in the current paper is that they are the results of statistical fluctuations. We summarize here the different (though not completely independent) tests that show that this would be a very unusual fluctuation indeed:

(1) Using method A and the power-law approximation for λ_Z there are fewer than five chances in 10^5 that all PF's would have had the same Λ as the primary beams.

(2) Using method B (i.e., the subset of interacting tracks only) and the same power law, both the mean of P_1 (one-link chains) and the corresponding likelihood curve strengthen this conclusion.

(3) We believe that, because of its freedom from assumptions about $\lambda(Z)$, the F test performed *at*

TABLE VI. Two-by-two table of the $P_2(Y)$ vs $P_2(X)$ scatter plot for two-link chains.

	$P_2(X)\le\frac{1}{2}$	$P_2(X)>\frac{1}{2}$
$P_2(Y)>\frac{1}{2}$	47	46
$P_2(Y)\le\frac{1}{2}$	75	47

fixed charge gives the strongest evidence for the fact that the mfp is shorter immediately after emission of a PF than at large distances. The chances for a statistical fluctuation are in this case about three in 10^4.

These highly implausible probability levels could be raised to quite acceptable values if we abandon the nh and assume that our PF's are infested by objects with an unexpectedly high reaction cross section. As was shown in Sec. V, one can fit on the data by assuming that 94% of PF's have λ_Z as given by the fit on primary beams and that 6% of PF's have $\lambda_a = 2.5$ cm, independent of Z. This λ_a corresponds to a conventional nuclear reaction cross section on the order of, or larger than, uranium.

Taken literally, the results imply the existence of a new state of multibaryonic matter with a hadronic reaction cross section two to ten times larger than the normal VOS nuclide of the same charge. However, before drawing such a far-reaching conclusion, we must exhaust all other avenues of interpretation.

B. Possible systematic effects and conventional explanations

The obvious suspicion is that the interpretation of this experiment may be influenced by systematic errors, by unappreciated conventional effects, or even combinations of these. We survey here those systematic and conventional effects that seem to us to be crucial for assessing the implications of our observations.

1. Measurement of distance

A trivial systematic, such as the incorrect assignment of interaction distances or potential paths, has been ruled out by internal checks and by remeasurements. Likewise, we have checked the data stream against the scanner's original notes and scan sheets. In every case, all computed quantities (such as S_N/N) were stable to at least four significant digits. The Monte Carlo simulation also incorporated the rounding of position coordinates to 100 μm units, as actually done at LBL, without pathological consequences.

2. Inhomogeneities in the emulsion

The possibility of gross defects or inhomogeneities in the emulsion composition itself must also be examined. The emulsion stacks used at LBL and NRC were manufactured at Ilford, Ltd., at different times; that both could be identically defective is unrealistic. Such gross defects would induce variations in sensitivity and affect the reproducibility of charge measurements, and especially the primary mfp. None of these effects were observed. Moreover, such effects would correlate with absolute positions in the plates, rather than relative distances after a star; this also was not seen.

3. Charge

An important question to address is whether or not a systematic error in the charge measurements would have affected the interpretation of the results. Obviously, this would systematically assign the measured mfp to the wrong charge Z; however, it would do so at all distances from the origin of the PF. We have made observational checks and Monte Carlo simulations to investigate the possible influence of such systematic effects on our conclusions. First, we observe that the charge measurements do not depend on distance from the emission point of a PF. Second, by Monte Carlo procedures, we introduced systematic shifts of 1, 2, and 3 charge units into the data. Although these shifts in charge do affect the absolute predicted mfp values for all charges, they indeed have no significant effect on the relative values of the measured mfp's.

For track lengths on the order of 1 mm or larger, the statistical error of 1 charge unit that was attained appears quite adequate for the requirements of this experiment on the basis of the Monte Carlo calculations. For shorter distances, the charge balance method was used, which requires detection of all relativistic singly charged tracks and correction for both meson production and charge exchange. Although the accuracy of charge measurements for distances < 1 mm is not known, one has the option to discard *all* track lengths (interacting or not) less than some cutoff distance from an interaction and examine the significance of the results after this cut. We have done this by selecting cutoff distances up to 5 mm and have found no changes in the conclusions from either the method *A* or *B* type of analysis.

4. Energy spectrum of PF's

Because the total reaction cross sections are remarkably constant for beam energies 0.87—

2.1A GeV,[16] the inclusion of PF's with energies as low as 0.5A GeV, for example, would have little effect on the measured mfp's. If anything, inclusion of low energy PF's would bias the data against a short mfp effect. Noting that the beam kinetic energy is $\sim 2A$ GeV, the energy-loss rates are at their minimum values. Hence, PF's with energies $\lesssim 2A$ GeV would necessarily have higher specific ionization and, as a result, would be assigned larger apparent charges. Such PF's would therefore be presumed to have mfp's shorter than their actual values. However, these considerations may not be of practical concern since ionization (charge) measurements made at various points along the tracks of PF's gave no evidence for a significant background of midrapidity PF's, as would be revealed by their increasing ionization rates with path length.

5. *Differential scanning efficiencies*

Another concern is the effect of a possible differential scanning efficiency. In this scenario, a short mfp could come about if an observer detects events more efficiently at short distances rather than at larger distances from a star. We note that in this experiment the "correct" mfp, i.e., the beam value, is observed at *large* distances and that an *excess* number of interactions is seen at short distances.

Any bias that is capable of reproducing Figs. 8 and 9 or Table III must be given serious consideration. One such obvious systematic is scanning bias, particularly a detection efficiency that is distance dependent.

Consider again the defining equation of the mfp

$$dN/dx = -N/\lambda \ . \tag{35}$$

If one imagines some small interval Δx in which one has incident N tracks, a perfect observer would detect $\Delta N = N(\Delta x/\lambda)$ interactions. An observer whose efficiency is ϵ $(0 < \epsilon \leq 1)$ would only observe $\Delta N' = \epsilon N(\Delta x/\lambda)$ interactions. Thus, in the presence of inefficiency, Eq. (35) is replaced by

$$dN/dx = -N(\epsilon/\lambda) \ . \tag{36}$$

This, of course, is identical to Eq. (35) with $\lambda' = \lambda/\epsilon$. Hence, all the analysis of Sec. IV proceeds through with this new λ'. This implies that a useful estimate of ϵ is $\epsilon^* = \lambda_R^*/\lambda^*$, where λ^* is the value obtained on the first scan, and λ_R^* is the value on the identical events after completing the rescan.

As mentioned earlier, LBL rescanned all events in which, on the initial scan, the primary Fe was observed to give rise to a secondary PF of charge ≥ 3. At NRC, tracks were reexamined by charge measurement; a "missed" interaction was located, in this method, whenever a new vertex with visible hadron emission was found by "backscanning" from the point where the change in charge of the PF was first detected.

We summarize the findings of the rescan in Table VII. Here, we give the values of Λ^* before the rescan and after the rescan for each laboratory as a function of the interaction distance of the PF, viz., within the first 2.5 cm after emission and at longer distances. The value of ϵ^*, the efficiency, is just the ratio of the Λ^* values before and after the rescan values. In the presence of a differential efficiency, we would have expected that the values of ϵ^* be distance dependent; as can be seen by inspection, they are not. LBL was $\sim 90\%$ efficient for a single scan, and NRC was $\sim 97\%$ efficient, normalized to the ultimate values obtained for each laboratory separately.

6. *Distance of confusion*

Owing to the high multiplicities of PF's within the forward fragmentation cone, it is conceivable that the interaction of PF's that occur at short distances from an interaction vertex actually occur before the ionization tracks of the PF's are visually resolved from each other. Under such circumstances charge measurements would be in error, as would the resultant estimates of λ_Z.

We have defined the confusion distance of a particular event to be the distance downstream from

TABLE VII. Observations on the number of interactions N and estimated value Λ^* on the first scan (indicated by 1 in the column headed Scan) and after the rescan (indicated by 2) for each laboratory in the two distance intervals. ϵ^* is the estimated scanning efficiency.

		$D \leq 2.5$ cm			$D > 2.5$ cm		
Laboratory	Scan	Λ^*	N	ϵ^*	Λ^*	N	ϵ^*
LBL	1	28.66	286		36.08	364	
	2	25.58	364		32.67	397	
				0.893			0.905
NRC	1	23.92	183		29.04	485	
	2	23.87	197		28.00	528	
				0.998			0.964

the interaction vertex beyond which *all* tracks emitted from the interaction are completely resolved. In emulsion, two particle tracks are visually resolved when separated by $1-2$ μm, depending on the charges of the particles. Figure 16 presents the distribution of confusion distances of PF's from a random sample of 1.88A GeV ^{56}Fe interactions. The distribution shows an exponential decrease at distances up to ~ 300 μm, with a negative logarithmic slope of about 100 μm as illustrated. The maximum confusion distance in this sample was ~ 1 mm, attributable to a pair of $Z=2$ PF's, quite possibly an example of the decay of a ^{8}Be fragment. We note that a confusion distance of ~ 1 mm is equal to the path length in emulsion necessary for colinear PF's at beam rigidity $R \approx 6$ GV to separate by ~ 1 μm through multiple Coulomb scattering alone.

We conclude that beyond $3-500$ μm, and certainly within 1 mm, virtually all PF's are effectively resolved, with charges and secondary interactions identifiable. These distances are 1 to 2 orders of magnitude less than $\lambda_a \approx 2.5$ cm that characterizes the short mfp component deduced from this experiment. As was done previously to reveal possible systematic errors in charge measurements, the elimination of all tracks of PF's (interacting or not) less than 5 mm in length should also suffice to eliminate the short mfp effect if it were attributable to nonresolved tracks. As mentioned above, we found no changes in the conclusions of our analysis before and after such path-length cutoffs were invoked.

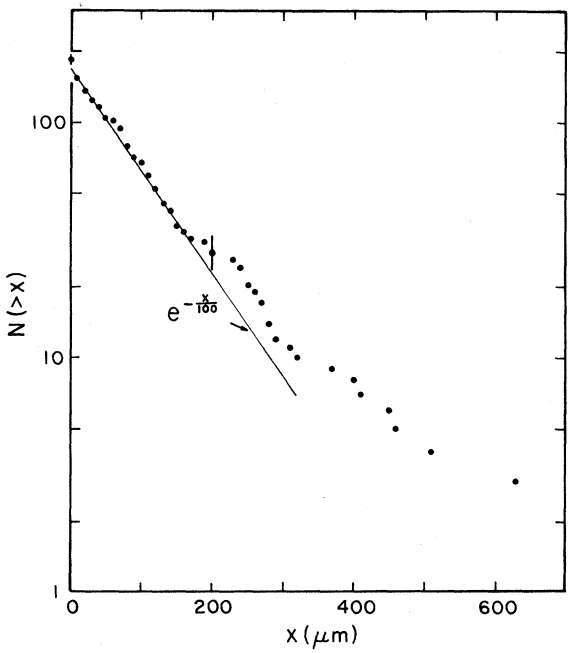

FIG. 16. Experimental integral distribution of the distance of confusion. The straight line corresponds to an exponential distribution with a mean distance of confusion of 100 μm.

7. *Background stars*

The sources of background stars are those attributable to random background from radioactive contamination (α decay), neutrons, and charged particles and to background correlated with the particular event under examination, from neutrons or, possibly, minimum ionizing tracks. A background event is one in which the path of a primary or PF track under investigation passes within ~ 2 μm from the vertex of a background star.

Such candidate background events would appear as stars with no noticeable change in charge and/or direction of the incident track. A direct estimate of the number of background events is made as follows: The typical density of all background stars in our emulsions exposed to ^{56}Fe in a volume ($10 \times 1.2 \times 0.6$ mm^3) centered on the primary track and located immediately downstream from primary interactions is ~ 1 star/mm^3. Taking the cross sectional area of an average ionization track to be ~ 4 μm^2, the total number of background events expected within the *first* cm of the primary Fe interactions (for ~ 3000 PF tracks) is about 0.1 events, about one-half of which would be recognized as due to natural radioactive α-decay chains by their characteristic ranges and be eliminated by the scanner. A background of events one order of magnitude greater than this estimate would still have a negligible effect on the conclusions of the experiment.

We may also test for the presence of background stars by a direct reference to our measurements on PF's. Consider the two-link topology. We define the charge change ΔZ to be the change in charge from the secondary to the tertiary at the secondary-tertiary vertex; e.g., if a secondary of charge 6 gives rise to a tertiary of charge 4, $\Delta Z = 2$. A background interaction as defined above must appear as a charge change $\Delta Z = 0$ or 1, the value 1 coming from our measured charge reproducibility, Fig. 3. As the maximum charge change in the NRC data used in this experiment was $8-3=5$, we restrict consideration of the LBL data to this same range of ΔZ as well. After this restriction, we divide the data into two classes: (i) $0 \leq \Delta Z \leq 1$ and (ii) $2 \leq \Delta Z \leq 5$. We compute the ratio R of the observed number of two-link chains to the number ex-

pected from the nh for class (i) and (ii). If we had a background-star problem, we would expect R for the two classes to differ and that R for class (ii), a class of events that is void of background, to have a value consistent with unity. However, we observe that R for class (i) equals 1.25 ± 0.09, while for class (ii) $R=1.29\pm0.10$. The fact that these two values are compatible and that neither is well accommodated if the nh is true (combining them, one has $\chi^2=16.5$, 2 DOF, which has a probability equivalent to 3.5 SD), allows us to conclude, as above, that we have no significant background contamination.

8. *Decays in flight: hyperfragments*

Perhaps the most obvious candidates to simulate nuclear interactions of PF's are decays in flight. Hyperfragment decay in flight is particularly appealing in that $c\tau\simeq3$ cm is comparable to hypernuclear decay lengths. We address the question of decays in flight from the data directly. Contributors to decay-in-flight topologies include hyperfragments and β-delayed proton emitters, as well as nuclear absorption of a π^- captured from an atomic orbit about the PF. In each of these cases, "decay products" have low velocities in the rest frame of the decaying object. Because $\gamma\simeq3$, all decay products must be relativistic in the laboratory frame; and since no target interactions are involved, "decay-in-flight" stars will in fact appear as projectile-fragmentation reactions with no associated target-related prongs, the so-called $N_h=0$ events. Noting that about 12% of primary beam interactions are of the $N_h=0$ type,[15] we may enquire whether or not there is an excess of $N_h=0$ stars among the PF's significantly above that expected for primary beam interactions. Such an excess could then be attributed to decays in flight.

Figure 17 is a microprojection drawing of the secondary and tertiary interactions initiated by an ^{56}Fe primary (schematically indicated) when *both* interactions are of the $N_h=0$ type. The kinematics of the decay of a hyperfragment at $\gamma=3.0$ are such that any emitted proton (pion) is restricted to a forward cone in the laboratory frame of 12° (16°); the minimum velocity of the proton (pion) emitted at 180° in the c.m. is $\beta_{\min}\approx0.83$ (0.78), which in this limiting case would be observed as a shower particle at 0° with grain density of 1.2 (1.3)$g_{\min}$. Consequently, all $|Z|=1$ products of hyperfragment decay in flight will appear as shower particles. Thus hyperfragment decay events at $\gamma=3$ would be restricted to the $N_h=0$ class of interactions, kinematically unable to simulate an interaction that involves the emission of low-energy target fragments.

To search for possible evidence within our data for excessive contributions due to decays in flight, we divided our data on the distribution of target-prong numbers N_h for PF interactions into two groups, $N_h=0$ and $N_h\geq1$ populated by n_0 and n_1 stars, respectively. We then examined the ratios $r=n_0/n_1$ for the cases when the interaction distances are $D\leq2.5$ and $D>2.5$ cm. Based on a subsample of 1189 PF stars, we observe the ratios

$$r\ (D\leq2.5)=0.13\pm0.02$$

and

$$r\ (D>2.5)=0.16\pm0.02\ .$$

The mean value of r for C, N, and O primary beams at 2A GeV is 0.15.

In the interval $D\leq2.5$ cm the number of PF interactions of all potential paths we observed is 590, 70 greater than expected for normal nuclei (i.e., the nh). Thus, if all this excess of events was hypothesized to be decays in flight ($N_h=0$ events), then the ratio r we would have expected to observe is $r=0.30$.

The values of r for $D\leq2.5$ cm are both in contradiction to the hypothesis of decays in flight, but are compatible with the value for primary beams. The conclusion we arrive at, then, is that the excess

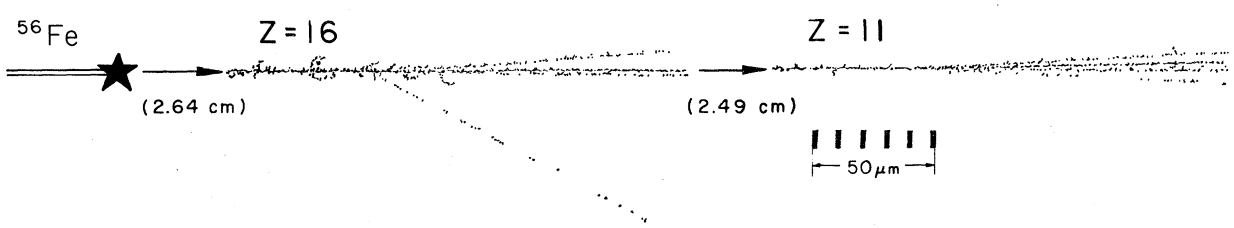

FIG. 17. Microprojection drawing of an ^{56}Fe interaction (schematically shown) that gives rise to secondary and tertiary PF interactions, both of which are of the $N_h=0$ type.

of interactions we see at distances $D \leq 2.5$ cm is not attributable to $N_h = 0$ events; hence this excludes the hypothesis of significant contributions to our data by hyperfragment (and other) decays in flight.

We have also estimated the abundance of relativistic hyperfragments in our data sample of PF's by referring to Refs. 25 and 26 for the measured, albeit approximate, production cross sections for free and bound Λ^0's in nuclear collisions. Based on most conservative approximations, we conclude that the fraction of PF's that could be hyperfragments is $\lesssim 10^{-3}$. The number of hyperfragment decays in flight contributing to the data is thus $\lesssim 3-5$, a number that, again, cannot account for the experimental observations.

9. *Conventional nuclei*

Last, as a conventional explanation of the apparent shortening of the mean free path, we consider isotopes and isomers with decay lengths $c\tau \sim 1$ cm.

(a) *Isotopes in the ground state.* We have already shown by means of the Monte Carlo simulation (Sec. IV C) that the predicted deviations of the isotopic cross sections from those at the VOS could not produce our effects.

(b) *Isomers.* Such nuclei might be assumed to have a larger reaction cross section; they would decay to the ground state either by channels that are very difficult to observe or would have decay-in-flight topologies that we have been able to exclude above (Sec. VI B *8*). To estimate the increase in cross section, we calculated the rms radii in the next shell model orbital excitation and then integrated the resulting density of nuclear matter to get relative excited state cross sections; we find that the changes in cross sections are generally less than 10%.

In contrast, the results of this experiment would require that $\approx 100\%$ of *all* PF's be produced with reaction cross sections $\gtrsim 20\%$ larger than the VOS nuclide of the same charge.[12] These cross sections must then return to VOS values with a mean decay length $c\tau \simeq 3$ cm to reproduce Fig. 8. Even this extreme assumption, unlikely as it is, fails to account for the memory effect (Sec. V.).

We now summarize this section:

(a) The comparison of mean free paths of projectile fragments at small and at large distances from the emission point (Figs. 11 and 8) rules out a homogeneous sample.

(b) Conventional explanations fail to account for our observations on the correlations between short tertiary links and short secondary links in two-link chains (Table VI), as well as for the results shown in Fig. 11.

(c) Systematic and background effects can be essentially eliminated by the observations themselves, e.g., normal mfp's observed at large distances from the emission point and no anomaly in the decay-in-flight topology at short distances.

10. *Implications*

We are thus left in a predicament. Conventional nuclear physics as well as systematics fail to explain the observations. The probability of a statistical fluctuation in this experiment is $\lesssim 5 \times 10^{-4}$.

In view of the fact that now two independent groups have reached essentially the same conclusions as we,[11,12] with comparable levels of confidence, the combined probability that the short mfp effect is a fluctuation becomes vanishingly small. The existence of at least one new type of multicharged, presumably multibaryon, state with a hadronic reaction cross section between two and ten times that of a VOS ground state nuclide of the same charge would explain the observations.

This simple model, involving one single kind of APF, quasistable over the distances observed here, is evidently not the only possible explanation. All or part of the $\Lambda^*(D)$ curve (Fig. 8), could, e.g., be due not only to removal of APF's by nuclear collisions with an enormous cross section, but also to removal by visually unobservable decay processes leading to a normal ground state nuclide.

Numerically, the following difficulties arise in such an alternative interpretation:

(i) A cross section "only" twice normal could be accommodated by the data, assuming, however, that *all* PF's are born as APF's ($\alpha \approx 1$) and that their mean decay length $c\tau$ is of the order of λ_a.

(ii) If the extreme assumption $\alpha = 1$ is abandoned, any $\alpha < 0.5$ will require again very large cross sections, which would produce a fast rise of the $\Lambda^*(D)$ curve even if $c\tau \gg \lambda_a$.

Recently, several speculative models suggesting new states of hadronic matter exhibiting properties akin to those of our hypothetical APF's have appeared in the literature.[27–30] To date, none of these models have yielded quantitative predictions for comparison with this experiment. New investigation addressing the obvious questions as to lifetimes, production, and interaction mechanism of the presumed APF component are in progress in our laboratories.

ACKNOWLEDGMENTS

The authors wish to thank the Bevalac operations staff for their many contributions to this experiment. We appreciate that considerable encouragement and support we have received from J. Cerny, H. Grunder, W. Hartsough, B. Harvey, and H. Pugh during the course of the experiment. We acknowledge the dedicated technical efforts of H. Dykman, J. Hodges, R. Smith, M. E. Stott, G. Williams, and H. Yee. We have benefited much from the discussions and constructive criticisms of our many colleagues. This work was supported in part by the Director, Office of Energy Research, Division of Nuclear Physics of the Office of High Energy and Nuclear Physics of the U. S. Department of Energy under Contract DE-AC03-76SF00098, and by the Deutsche Forschungsgemeinschaft and NATO.

APPENDIX A

A. Distribution of the total path length

Given the probability density for one track length X_i in an infinite detector

$$f_1(X_i)=\frac{1}{\lambda}e^{-X_i/\lambda}\ , \tag{A1}$$

we seek the probability density for the sum of N such X values

$$S_N\equiv\sum_{i=1}^{N}X_i\ , \tag{A2}$$

i.e., the N-fold convolution of densities given by Eq. (A1). This is by definition

$$f(S_N)=\int\theta(X_1)\cdots\int\theta(X_N)\theta(S_N)\delta\left[S_N-\sum_{i=1}^{N}X_i\right]\prod_{i=1}^{N}\frac{dX_i}{\lambda}e^{-X_i/\lambda}\ . \tag{A3}$$

Here the θ functions ensure that all lengths are positive and the δ function represents the constraint (A2). Thus, e.g., for $N=2$ one obtains by elementary integration

$$f(S_2)=\frac{1}{\lambda}\frac{S_2}{\lambda}e^{-S_2/\lambda}\ . \tag{A4}$$

For the general case the folding is most easily performed by means of moment generating functions (mgf) $G_u(t)$, where u is either X_i or S_N. By definition

$$G_{X_i}(t)\equiv\int_0^\infty e^{tX_i}f_i(X_i)dX_i=\frac{1}{1-\lambda t}\ . \tag{A5}$$

For a folding of N independent variables one has

$$G_{S_N}(t)=\prod_{i=1}^{N}G_{Xi}(t)=\frac{1}{(1-\lambda t)^N}\ , \tag{A6}$$

since all X_i have the same probability density (A1) and hence the same mgf (A5).

Taking the inverse Laplace transform of Eq. (A6) we obtain Eq. (7).

B. Conversion of path-lengths S into χ^2 variates

Let

$$y_i\equiv\frac{2X_i}{\lambda}\ . \tag{A7}$$

The mgf for y is then

$$G_{y_i}(t)=\int_0^\infty e^{ty}e^{-y/2}\frac{dy}{2}=\frac{1}{1-2t}\ . \tag{A8}$$

Replacing S_N, Eq. (A2) by

$$h^2=\frac{2S_N}{\lambda}\ , \tag{A9}$$

we obtain the mgf for h^2

$$G_{h^2}(t)=\frac{1}{(1-2t)^N}\ . \tag{A10}$$

The meaning of h^2 becomes evident if we invoke the properties of normal deviates. Let Z_j be a normal deviate of zero mean and unit variance. The mgf for *the square of* Z_j is then

$$G_{Z_j^2}(t)=\frac{1}{(1-2t)^{1/2}}\ , \tag{A11}$$

and that of any sum of ν such squares

$$\chi^2\equiv\sum_{j=1}^{\nu}Z_j^2 \tag{A12}$$

is

$$G_{\chi^2}(t)=\frac{1}{(1-2t)^{\nu/2}}\ . \tag{A13}$$

Identifying Eqs. (A10) and (A13) we see that h^2, i.e., $2S_N/\lambda$, is indeed a χ^2 variate; since $N=\nu/2$,

$2S_N/\lambda$ is χ^2 distributed with $2N$ degrees of freedom, Q.E.D.

An advantage of the change of variables from S_N to h^2 lies in the fact that the probability density

$$W(h^2)=[2^N\Gamma(N)]^{-1}(h^2)^{N-1}e^{-h^2/2} \tag{A14}$$

and its CDF

$$P_S(h^2)=\int_0^{h^2} W(t)dt \tag{A15}$$

are well tabulated and adequate algorithms for computers are available (see, e.g., Ref. 22).

C. Distribution of the ratio F

Another important consequence of the χ^2 distribution of $2S_N/\lambda$ is the possibility to reduce the comparison of two λ^* values to a well-known distribution law. Indeed, the ratio F can be rewritten as follows (in obvious notation):

$$F\equiv\frac{\lambda_1^*}{\lambda_2^*}=\frac{S_{N_1}/N_1}{S_{N_2}/N_2}=\left[\left[\frac{2S_{N_1}}{\lambda}\right]\Big/\left[\frac{2S_{N_2}}{\lambda}\right]\right]\frac{N_2}{N_1}$$
$$=\left[\frac{h_1^2}{2N_1}\right]\Big/\left[\frac{h_2^2}{2N_2}\right]. \tag{A16}$$

As is well known (see, e.g., Ref. 22), the ratio of two χ^2 deviates, each divided by their number of degrees of freedom (ν_1 and ν_2) obeys the so-called F (or variance ratio) distribution, commonly used in variance analysis. Its probability density is

$$W(F)=\frac{\nu_1^{\nu_1/2}\nu_2^{\nu_2/2}}{B\left[\frac{\nu_1}{2},\frac{\nu_2}{2}\right]}F^{(\nu_1-2)/2}(\nu_2+\nu_1F)^{-(\nu_1+\nu_2)/2}, \tag{A17}$$

where B is the beta function. Identifying the numbers of degrees of freedom ν_1 and ν_2 with $2N_1$ and $2N_2$, respectively, we obtain the integral probability (CDF) of F given in Eq. (15).

Figure 18 shows an example of the F distribution, for the case of $Z=11$ secondaries in the LBL sample, where 15 interactions were recorded before $D=2.5$ cm, and 12 beyond.

The expected mean value of F is $N_2/(N_2-1)$; the mode of the distribution lies at

$$N_2(N_1-1)/N_1(N_2+1)\,.$$

Both values are indicated on the graph along with the median value computed from Eq. (15) [setting $P(<F)=\frac{1}{2}$]. The observed value of F, $F_{\rm obs}$, is shown together with (the shaded area) the integral $P\,(<F_{\rm obs})$.

D. Chi-squared test in method A'

We construct a goodness of fit test for comparing a set of mfp values using the "traditional" concept of the χ^2 test. Let S_N with N stars be the total sample, so that $\bar{\lambda}=S_N/N$. Let the sample be divided into M subsamples, say s_i and n_i, $i=1$ to M. For each value s_i, construct $Z_i^2\equiv 2s_i/\lambda$, which is distri-

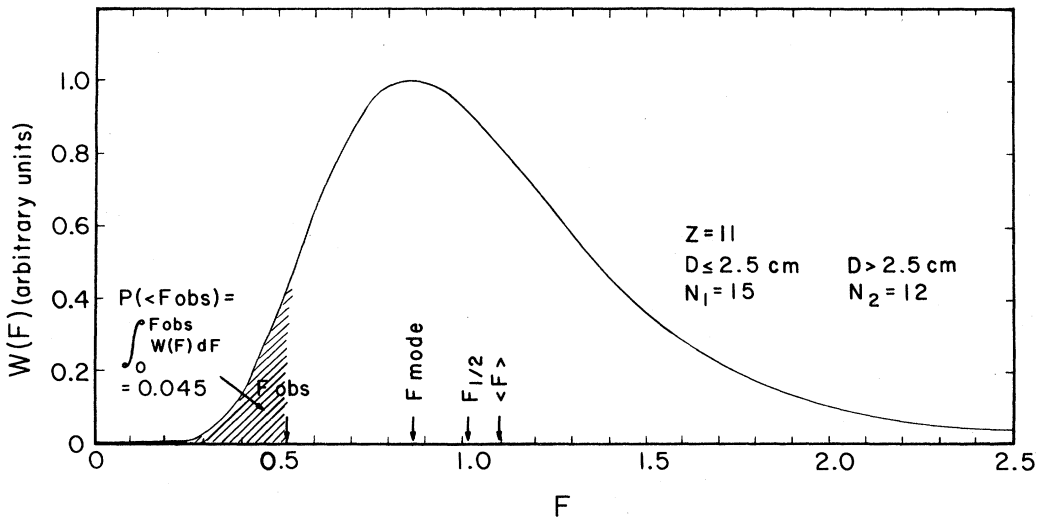

FIG. 18. Shape and characteristic values of a typical F distribution expected for the case of $Z=11$ PF's in the LBL (^{56}Fe) sample.

buted χ^2 with $2n_i$ DOF. We calculate then the integral probability p_i of the Z_i distribution, Eq. (A15). For each p_i we compute that value of a normal deviate ξ_i that has the same one-sided integral probability p_i. Now let

$$q^2=\sum_{i-1}^{M}\xi_i^2 .$$

Assuming the values s_i,n_i to come from a population with the same mfp λ, q^2 is distributed like χ^2 with $M-1$ DOF. This is what we did, for example, when we reported in Sec. V A that the NRC primary ^{16}O measurements of the mfp, plotted as a function of distance after pickup (Fig. 7), are fit by a constant mfp λ. We point out that the properties of the χ^2 distribution were used by us in two other contexts in Secs. IV A and B and subsections A and B of Appendix A.

E. Differential equations governing the two-link chain topology

We give here the explicit differential equations that can be integrated to give the probability densities used in Sec. IV B.

$$\frac{dN_1}{dZ}=\frac{-N_1}{\lambda_X},$$
$$\frac{dN_2}{dZ}=\frac{-N_2}{\lambda_y}+\frac{N_1}{\lambda_X}, \qquad \text{(A18)}$$

where N_1 is the number of tracks of generation i and N_2 is the number of tracks of generation $i+1$, e.g., N_1 and N_2 refer to secondary and tertiary tracks, respectively.

APPENDIX B

A. Monte Carlo simulation of detector response

One other feature was incorporated into the Monte Carlo simulation that deserves mention. If one calculates *a priori* expected mfp's based on geometrical cross sections in emulsion, without normalizing to any observed emulsion mfp, one soon discovers that the predicted mfp's are much shorter than the observed ones, including the observations on primary VOS beams. This is due mainly to detector inefficiencies and in part also observer inefficiencies for certain channels, particularly quasielastic reactions at low momentum transfer. One can prove mathematically that if one misses a constant fraction p of events with a mfp λ_{th} (the theoretical unnormalized mfp), the observed mfp $\lambda=\lambda_{th}/(1-p)$ and the measured X values will again obey an exponential law.

To simulate this situation, a value of $p=\frac{1}{2}$ was actually assumed, i.e., emulsion was considered only 50% efficient. After having the program assign a mfp as explained above (including charge assignment and isotopic effects), this value was divided by two and then an SID was generated. If this distance were within the stack, another random number was generated. If it were less than 0.5, a "visually detected" interaction was assumed to have occurred; if not, another random interaction distance using the same $\lambda/2$ was generated and the program proceeded in like fashion until the track suffered a detected interaction or left the stack.

APPENDIX C

A. Further implications of the two-link chain topology

We now examine the $P_2(X)$ vs $P_2(Y)$ unit plane in further detail by referring to Figs. 19(a) and (b). In Fig. 19(a), we have divided the $P_2(Y)$ sample into two parts, the first for which $P_2(X)\leq\frac{1}{2}$ [area (a)] and the other for which $P_2(X)>\frac{1}{2}$ [area (b)]. Similarly, we have divided the $P_2(X)$ sample into two parts for which $P_2(Y)\leq\frac{1}{2}$ [area (d)] and $P_2(Y)>\frac{1}{2}$

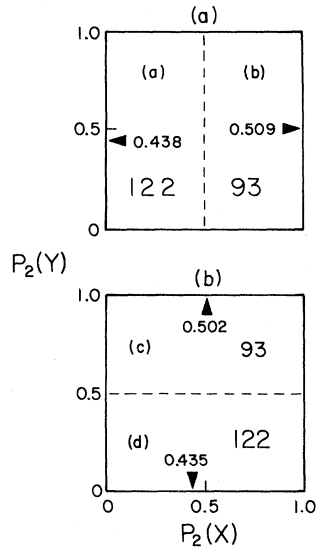

FIG. 19. Asymmetry plots on the $P_2(X)$ vs $P_2(Y)$ unit plane.
(a) $P_2(Y)$ selected by $P_2(X)$.
(b) $P_2(X)$ selected by $P_2(Y)$.

[area (c)], Fig. 19(b). Because $P_2(Y)$ is independent of $P_2(X)$, and *vice versa,* under the nh we expect the means of all the samples of P_2 to be $\frac{1}{2}$.

Taken at face value, the interpretation of the data as presented in Figs. 19(a) and (b) leads to several qualitative conclusions. For mnemonic as well as for physical reasons, we shall denote $P \leq \frac{1}{2}$ as short and $P > \frac{1}{2}$ as normal. This notation alludes to the fact that short X or Y values correspond to events enriched in APF's, whereas the normal X or Y values are depleted in APF's, and hence should behave more like a beam of normal nuclei.

First, let us consider areas (a) and (d), where we note the following:

(i) if $P_2(X) \leq \frac{1}{2}$ (short), then $\bar{P}_2(Y)=0.438$ (122 stars);

(ii) if $P_2(Y) \leq \frac{1}{2}$ (short), then $\bar{P}_2(X)=0.435$ (122 stars).

In these cases, the selection of events having a short X (Y) link results in a short Y (X) link, in that both the $P_2(Y)$ and $P_2(X)$ values are $< \frac{1}{2}$. Item (i) is a restatement of the result from Sec. V B that a short PF parent gives rise to a short PF progeny (memory). Second, consider areas (b) and (c), where we see that

(iii) if $P_2(X) > \frac{1}{2}$ (normal), then $\bar{P}_2(Y)=0.509$ (93 stars);

(iv) if $P_2(Y) > \frac{1}{2}$ (normal), then $\bar{P}_2(X)=0.502$ (93 stars).

In other words, the selection of events with a normal $X(Y)$ link leads to normal $P_2(Y)$ and $P_2(X) \simeq \frac{1}{2}$ values. We have therefore extracted a subsample of the two-link chain data that exhibit normal behavior. This result speaks against isotopic and related conventional nuclear physics effects, for if these were the root cause of the short-mfp effect one would expect that $\bar{P}_2 \neq 0.5$ in both instances. Too, even though the fit of beam mfp's to a power-law expression cannot be exact, the PF data do not categorically reject such a fit, as one symptom of a rejection would be $\bar{P}_2 \neq \frac{1}{2}$.

A third observation is that for case (iii), the fact that $P_2(Y)=0.509$ does not differ significantly from $\frac{1}{2}$ indicates that the seemingly normal $P_2(X) > \frac{1}{2}$ secondary population does not seem to produce anomalous tertiaries as copiously as do normal primaries [where $\bar{P}_1(X)=0.469$; Fig. 12]. If this is not simply a statistical fluctuation (see Table VI), one possible explanation for this observation would be the existence of an energy threshold for APF production. A similar energy dependence is also suggested by Judek's cosmic-ray observations.[6]

[1]A. Milone, Nuovo Cimento Suppl. 12, 353 (1954).

[2]H. Yagoda, Bull. Am. Phys. Soc., Series II, 64 (1956); Nuovo Cimento 6, 559 (1957).

[3]S. Tokunaga, T. Ishii, and K. Nishikawa, Nuovo Cimento 5, 517 (1957).

[4]H. Bradt and B. Peters, Phys. Rev. 77, 54 (1950).

[5]E. M. Friedlander and M. Spirchez, *International Working Meeting on Cosmic Rays* (Romanian Academy of Science, Bucharest, Romania, 1959), p. 155; Nucl. Sci. Abstr. 15, 347 (1961).

[6]B. Judek, Can. J. Phys. 46, 343 (1968); 50, 2082 (1972).

[7]T. F. Cleghorn, P. S. Freier, and C. J. Waddington, Can. J. Phys. Suppl. 46, 572 (1968).

[8]B. Judek, in *Proceedings of the Fourteenth International Conference on Cosmic Rays, 1975,* edited by Klaus Pinkau (Max-Planck-Institute, Munchen, 1975), Vol. 7, pp. 2342 and 2349.

[9]We have adopted the notation for kinetic energy suggested by A. S. Goldhaber and H. H. Heckman, Annu. Rev. Nucl. Part. Sci. 28, 161 (1978).

[10]E. M. Friedlander, R. W. Gimpel, H. H. Heckman, Y. J. Karant, B. Judek, and E. Ganssauge, Phys. Rev. Lett. 45, 1084 (1980).

[11]P. L. Jain and G. Das, Phys. Rev. Lett. 48, 305 (1982).

[12]H. B. Barber, P. S. Freier, and C. J. Waddington, Phys. Rev. Lett. 48, 856 (1982).

[13]C. F. Powell, P. H. Fowler, and D. H. Perkins, *The Study of Elementary Particles by the Photographic Method* (Pergamon, London, 1959).

[14]W. H. Barkas, *Nuclear Research Emulsions* (Academic, New York, 1963), Vol. I.

[15]H. H. Heckman, D. E. Greiner, P. J. Lindstrom, and H. Shwe, Phys. Rev. C 17, 1735 (1978), and this work.

[16]J. Jaros, A. Wagner, L. Anderson, O. Chamberlain, R. Z. Fuzesy, J. Gallup, W. Gorn, L. Schroeder, S. Shannon, G. Shapiro, and H. Steiner, Phys. Rev. C 18, 2273 (1978); see also Ref. 15.

[17]P. J. Karol, Phys. Rev. C 11, 1203 (1975); values for the parameters were obtained from Ref. 15.

[18]We recently obtained partial confirmation of this prediction by measurements on beams of ^{6}Li and ^{3}He (unpublished).

[19]D. E. Greiner, P. J. Lindstrom, H. H. Heckman, B. Cork, and F. S. Bieser, Phys. Rev. Lett. 35, 152 (1975). Note that these results were not reported in the laboratory frame, so that a Lorentz transformation is involved to obtain the result quoted.

[20]A publication on this δ-ray technique for measuring charge is in preparation.

[21]M. S. Bartlett, Philos. Mag., Ser. 7 44, 249 (1953).

[22]M. Abramovitz and J. A. Stegun, *Handbook of Mathematical Functions* (Dover, New York, 1970), p.

925.

[23]Anomalous particle fragments are sometimes called "anomalons."

[24]Hereafter $\hat{\Lambda}$ is the maximum likelihood estimate within the context of method *B*, not to be confused with Λ^*, Eq. (12).

[25]K. J. Nield, T. Bowen, G. D. Cable, D. A. DeLise, E. W. Jenkins, R. M. Kelback, R. C. Noggle, and A. E. Pifer, Phys. Rev. C 13, 1263 (1976).

[26]J. W. Harris, A. Sandoval, R. Stock, H. Stroebele, R. E. Renfordt, J. V. Geaga, H. G. Pugh, L. S. Schroeder, K. L. Wolf, and A. Dacal, Phys. Rev. Lett. 47, 229 (1981).

[27]Y. Karant, Lawrence Berkeley Laboratory Report LBL-9171, 1979.

[28]W. J. Romo and P. J. Watson, Phys. Lett. 88B, 354 (1979).

[29]H. Stöcker, G. Graebner, J. A. Maruhn, and W. Greiner, Phys. Lett. 95B, 192 (1980).

[30]S. Fredriksson and M. Jändel, Phys. Rev. Lett. 48, 14 (1982).